Final Report

09/2025

Student Project No. [AHDB project number]

Title: Genetic Manipulation of Stomatal Patterning and Behaviour to Optimise Gas Exchange in the Cultivated Strawberry

[William Atkinson[1]], [Andrew J. Simkin[1]] and [Tracy Lawson[2]]

[1] [University of Essex]
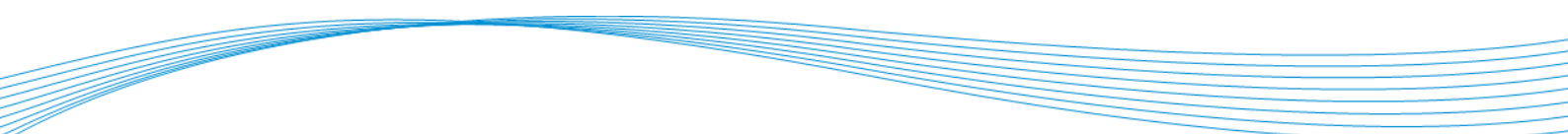
[2] [University of Illinois Urbana-Champaign]

Supervisors:

Dr. Andew Simkin, Dr. Graham Dow and Prof. Tracy Lawson

Report No: [AHDB Use only]

Notes:

- *Website:*

Please note that this document will be made available through AHDB's website. If you need us to delay publication due a peer review in a publication or journal, please notify us.

The Industry Summary will be used to populate the project webpage and to inform AHDB knowledge exchange and communications; please be mindful of the target audience (famers, levy payers and industry stakeholders).

- *Commercial sensitivity:*

If the final report needs to be held back due to commercial sensitivity, please advise your AHDB Research Manager who will supply you with a template for an abridged version by way of web summary holding document.

- *Please try and keep this document to a maximum of 50 pages in length (excluding appendices).*

Table of Contents

1. Industry Summary

Strawberry production is highly sensitive to water use and photosynthetic efficiency, both of which are controlled by stomata—the pores on the leaf surface. This research tested whether modifying stomatal traits could improve gas exchange and productivity in cultivated strawberry.

Why was this work important?

- Strawberries often face midday limitations in photosynthesis due to stomatal closure, which restricts CO_2 uptake and reduces yield potential.

- Improving stomatal performance is a promising way to increase productivity and water-use efficiency without changing cultivation practices.

Key findings and conclusions:

- **Constitutive overexpression of STOMAGEN** (a positive regulator of stomatal development) successfully increased stomatal density, raising the potential for greater CO_2 uptake.

- **Guard cell-specific expression of Hexokinase (HXK1)** promoted earlier and stronger stomatal closure in response to sugars, leading to reduced water loss without reducing photosynthesis.

- Combining both traits in strawberry showed how developmental (stomatal number) and metabolic (guard cell regulation) approaches can be used together to tune gas exchange.

Practical outputs and outcomes:

- Demonstrated proof-of-concept that manipulating stomatal traits can improve gas exchange balance in strawberry.

- Provided new genetic targets (STOMAGEN and guard-cell HXK1) for breeding and biotechnology programs.

- Highlighted trade-offs between higher stomatal density (increased CO_2 uptake) and tighter closure (improved water-use efficiency), showing the need for balanced deployment in field conditions.

Who will benefit and why?

- **Growers**: Potential access to strawberry varieties with improved productivity under fluctuating light and water-limited conditions.

- **Breeders**: New trait targets to integrate into breeding pipelines.

- **Industry stakeholders**: Improved resource-use efficiency could reduce irrigation costs and support sustainability goals in strawberry production.

2.   Introduction

Strawberry (Fragaria × ananassa) is a high-value horticultural crop with global economic importance. However, its productivity is often constrained by limitations in photosynthesis, particularly under variable environmental conditions. One of the primary factors influencing photosynthetic efficiency is stomatal behaviour, which regulates the balance between CO_2 uptake and water loss.

Stomata are controlled both by their **developmental traits** (such as number and distribution) and by **guard cell metabolism**, which determines their responsiveness to internal and external signals. Previous research has shown that:

- Increasing stomatal density can raise the anatomical maximum conductance, improving CO_2 uptake and photosynthetic capacity.
- Modifying guard cell metabolism, such as through sugar sensing via hexokinase, can enhance stomatal responsiveness and improve water-use efficiency.

Despite these insights, there has been limited work applying these strategies directly to strawberry, where stomatal limitation is a significant bottleneck to yield.

Objectives of this project were to:

- Test the effect of **constitutive overexpression of STOMAGEN** to increase stomatal density.
- Evaluate **guard cell-specific expression of Hexokinase (HXK1)** to improve stomatal closure and reduce water loss.
- Assess the combined impact of these modifications on **gas exchange, photosynthetic performance, and plant productivity** in strawberry.

This research provides an abridged scientific record of the experiments undertaken and the rationale behind using both developmental and metabolic targets to optimise stomatal function. A full record of methods and data is available in the accompanying thesis.

3. Materials and methods

3.1. Construct Assembly

3.1.1. Module design

All synthesised Level 0 modules were designed and codon optimised for expression. The *Arabidopsis thaliana* sequence for Stomagen was obtained from Tanaka et al. (2013) (Tanaka *et al.*, 2013). The *Arabidopsis thaliana* sequence for Hexokinase 1 was taken from Kelly et al. (2013) (Kelly *et al.*, 2013). The *Arabidopsis thaliana* sequence for Arabidopsis H+ATPase 2 (AHA2) was obtained from Wang et al. (2013) (Wang *et al.*, 2013). Codons were optimised for expression in dicots (*Nicotiana tabacum*) and to remove restriction sites for the enzymes used in GoldenGate cloning (BsaI and BbsI) using the Vector Builder Codon Optimisation Tool (Vector Builder, www.VectorBuilder.com)

3.1.2. Level 0 modules synthesis and preparation

Level 0 modules were synthesised by NBS Biologicals (NBS Biologicals, UK). Level 1 destination vectors, the assembled Kanamycin resistance Level 1 module and the Level 1 and 2 linkers were provided by the University of Essex (University of Essex, UK). The Level 2 destination vector was provided by Niab (Niab, UK).

3.1.3. Assembly of Level 1 modules

Level 1 constructs were assembled from Level 0 using the Golden Gate modular cloning method established by Weber *et al.*, 2011 (Weber *et al.*, 2011). 1 μL Level 1 destination vector (100 ng μl^{-1}), 1 μL of each Level 0 (containing the selected promoter, coding sequence, and terminator) (100 ng μl^{-1}), 1.5 μL of 10x NEB T4 buffer, 1.5 μl of 10x BSA, 1 μL NEB T4 DNA Ligase. Each reaction also contained 1 μL of the level-specific restriction enzymes BsaI and dH$_2$O to bring the reaction volume to 15 μL. The digestion and ligation were performed in a thermocycler

using the following program: 25x cycles of 37 °C for 3 minutes and 16 °C for 4 minutes, 1x cycle of 50 °C for 5 mins and 1x cycle of 80 °C for 5 mins.

A.

B.

C.

D.
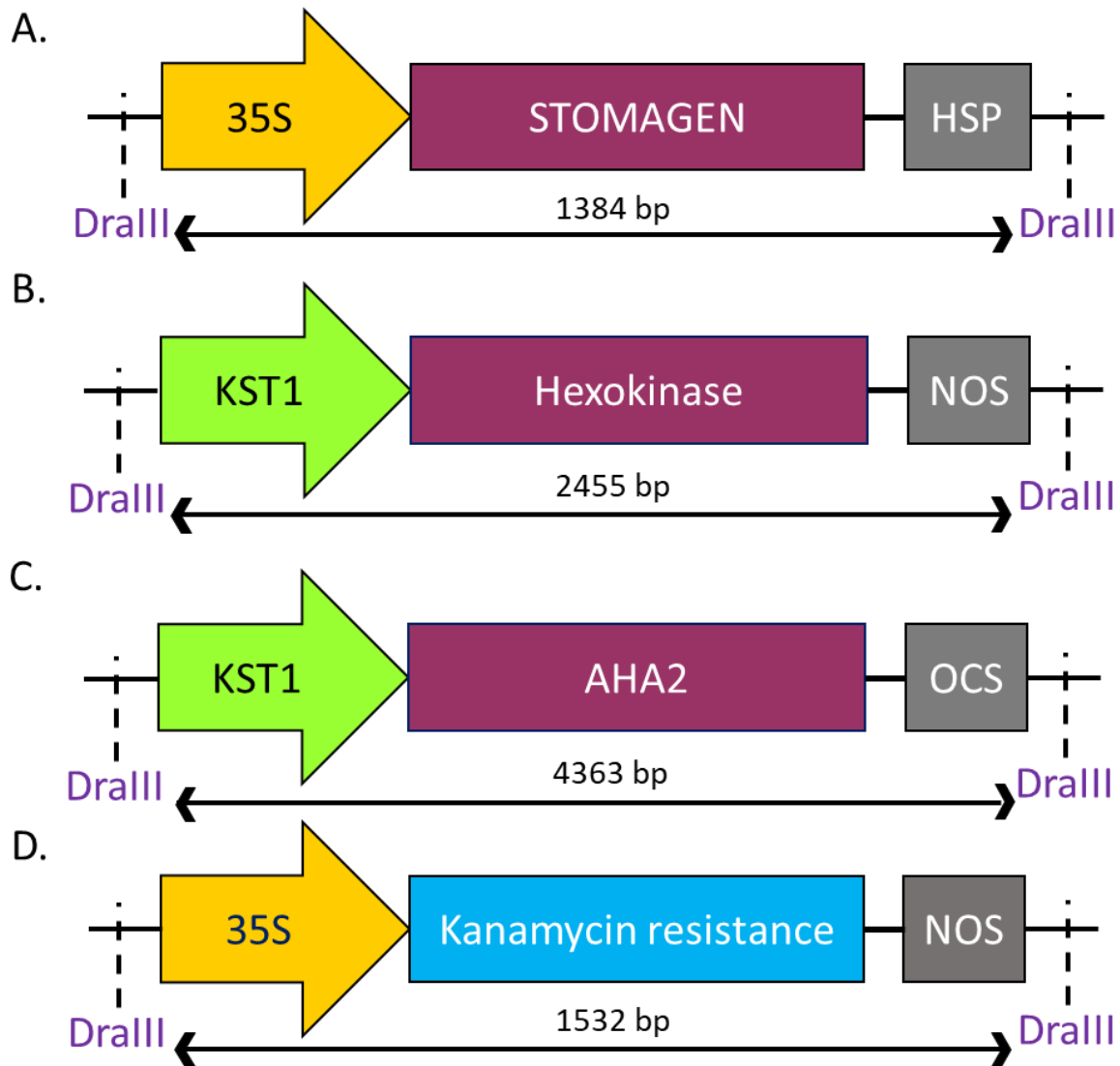
Figure 2.1. Schematic representation of assembled Level 1 modules. Figure 2.1A depicts STOMAGEN under the control of the CaMV35S constitutive promoter and the Heat Shock Protein (HSP) terminator. Figure 2.1B depicts Hexokinase under the control of the Solanum tuberosum Guard cell-specific promoter KST1 and the nolapine synthase (NOS) terminator. Figure 2.1C depicts AHA2 under the control of the Solanum tuberosum Guard cell-specific promoter KST1 and the nolapine synthase (OCS) terminator. The insert site is flanked by DraIII restriction enzyme recognition sites, and the arrows depict the length of the insert.

3.1.4.   Bacterial transformation and colour selection

Following the assembly of Level 1 constructs, chemically competent *E. coli* cells (in-house-made DH5α cells) were transformed with each of the Golden Gate modules (Fig. 2.1) using the heat shock method of transformation (Froger and Hall, 2007). 4 µL of each Golden Gate module (100 ng µL^{-1}) was added to ice-thawed chemically competent E. coli cells (Top10 Thermo Fisher Scientific or in-house-made DH5α cells) and were tap mixed. The cells were placed on ice for 2 minutes before being transferred to a water bath/ heating block at 42 °C for 45 seconds, then immediately returned to the ice for an additional 2 minutes. 300 µL of Super Optimal Broth (SOB) was added to the cells, and they were left to incubate for 1 hour at 37 °C. After the incubation period, the cells were well mixed with a pipette before adding 100 µL of the broth to agar plates. Cells were grown on agar plates containing ampicillin (100 µg mL^{-1}), supplemented with X-gal and IPTG (1.5 µL mL^{-1}) to permit blue/white selection of colonies. Cells were incubated overnight at 37 °C. White colonies containing the putatively correctly assembled Level 1 module were isolated.
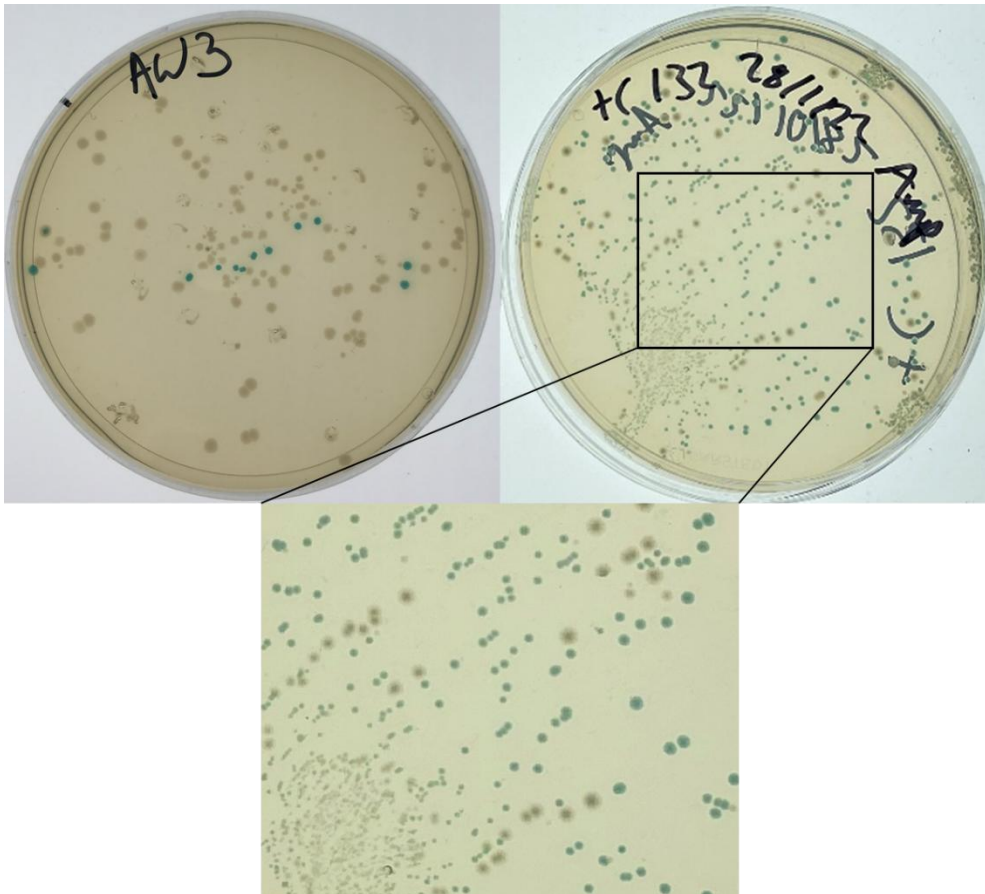
Figure 2.2. Blue/white selection of E. coli cells containing assembled Level 1 Golden Gate modules. Blue colonies contain only the Level 1 destination vector. White colonies contain the Level 1 destination vector with the inserted Level 0 modules. Figure 2. ▣ shows a blue/white selection of E. coli cells containing an assembled Level 1 construct. Figure 2.2B represents a control, displaying colonies containing the Level 1 destination vector 132, which still contains the Lac operon.

3.1.5.   Plasmid isolation and quantification

Three independent colonies displaying the desired white phenotype were selected (Fig. 2.2). Overnight cultures of isolated single white colonies, collected using the colony picking method, were made and incubated overnight in approximately 5 mL of high salt LB broth containing 100 µg mL^{-1} of ampicillin (100 µg mL^{-1}) as a selectable marker.

Plasmids were extracted using a NucleoSpin® plasmid kit (Machery-Nagel) following the manufacturer's instructions, using sterile Milli-Q® Ultrapure water instead of the elution buffer.

Extracted plasmid concentrations were measured using Nanodrop 1000 (ThermoFisher Scientific).

Extracted plasmids were diluted to 100 ng µL^{-1} for further Golden Gate assemblies.

Level 1 plasmids were subject to DraIII restriction enzyme digestion to ensure correct assembly. The Level 1 vectors contain the restriction site CACNNNGTG for DraIII digestion. 17 µL of plasmid was incubated with 1 µL of DraIII and 2 µL of 10x rCutsmart buffer for 1 hour at 37 °C. Samples were run on a 1% agarose gel at 160 volts for 1 hour. Banding patterns were compared to the known sizes of the digested plasmid to confirm correct assembly.
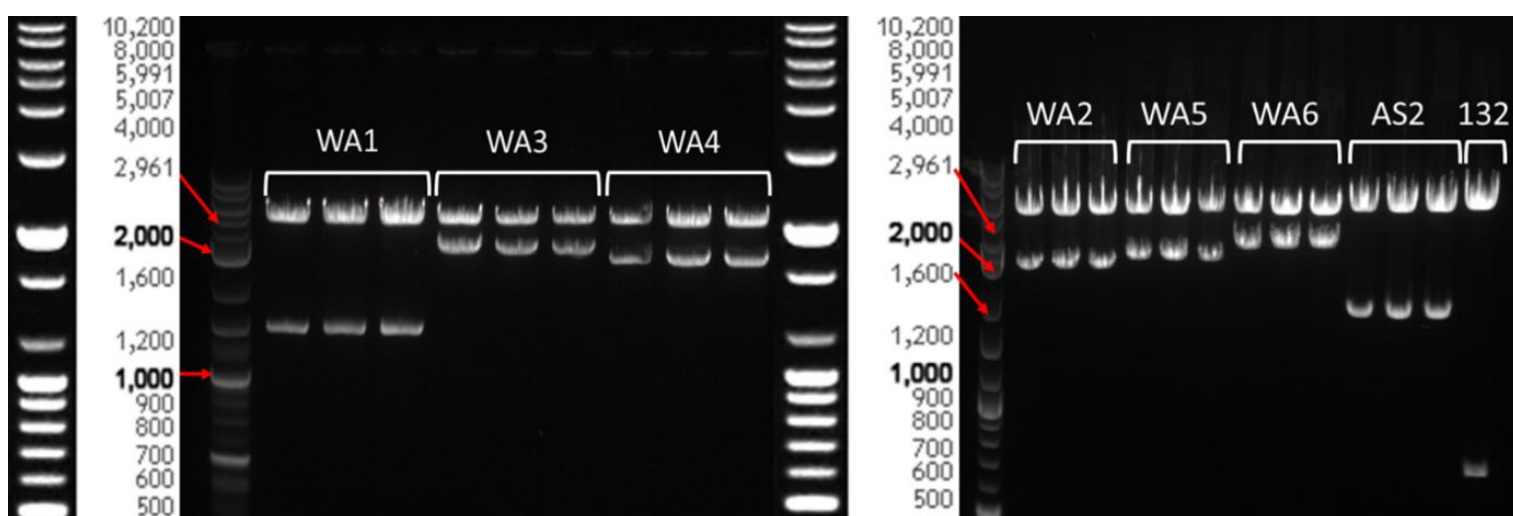
Figure 2.3. DraIII digestion of extracted plasmid from single colonies post-blue/white selection. The red arrows show the respective bands on the ladder. WA1 and WA2 represent the Level 1s depicted in Figure 2.1A and B. WA3 and 4 represent backup Level 1 constructs for Guard cell-specific overexpression of Hexokinase using an alternative ADP-Glucose Pyrophosphorylase promoter. WA5 and 6 represent the Level 1 constructs for Guard cell-specific overexpression of Hexokinase in position 3 for multigene assembly, using ADP-Glucose Pyrophosphorylase and KST1 promoters, respectively. AS2 represents Guard cell-specific overexpression of a MADS box transcription factor for an additional project. The arrows highlight the corresponding bands from the digestion chart to the left. The digestion of 132, the level 1 destination vector, acts as a positive control.

3.1.6.   Assembly of Level 2 modules

Level 1 plasmids displaying the correct banding patterns were used for Level 2 assembly. Level 2 constructs were assembled as described in section 2.1.3 using the restriction enzyme BbsI, replacing BsaI. Following Golden Gate assembly as described (section 4.1.2), NEB® 10-beta Competent *E. coli* (High Efficiency) were transformed with 4 µL of each Level 2 assembly as

described above. Cells were plated onto agar plates using kanamycin (100 µg mL^{-1}) for selection and incubated overnight at 37 °C.

Bacterial transformation and colour selection were carried out as described above. In brief, *E. coli* cells were transformed with the assembled Level 2 construct and were visually discriminated using red/white colour selection (Figure 2.4). Colonies presenting a red phenotype (Figure 2.4A) contain only the Level 2 destination vector with the still intact canthaxanthin biosynthesis operon. Following assembly, the canthaxanthin operon is replaced by the integration of the level 1 modules, resulting in white colonies (Figure 2.4B). White colonies were selected and had their plasmids extracted.
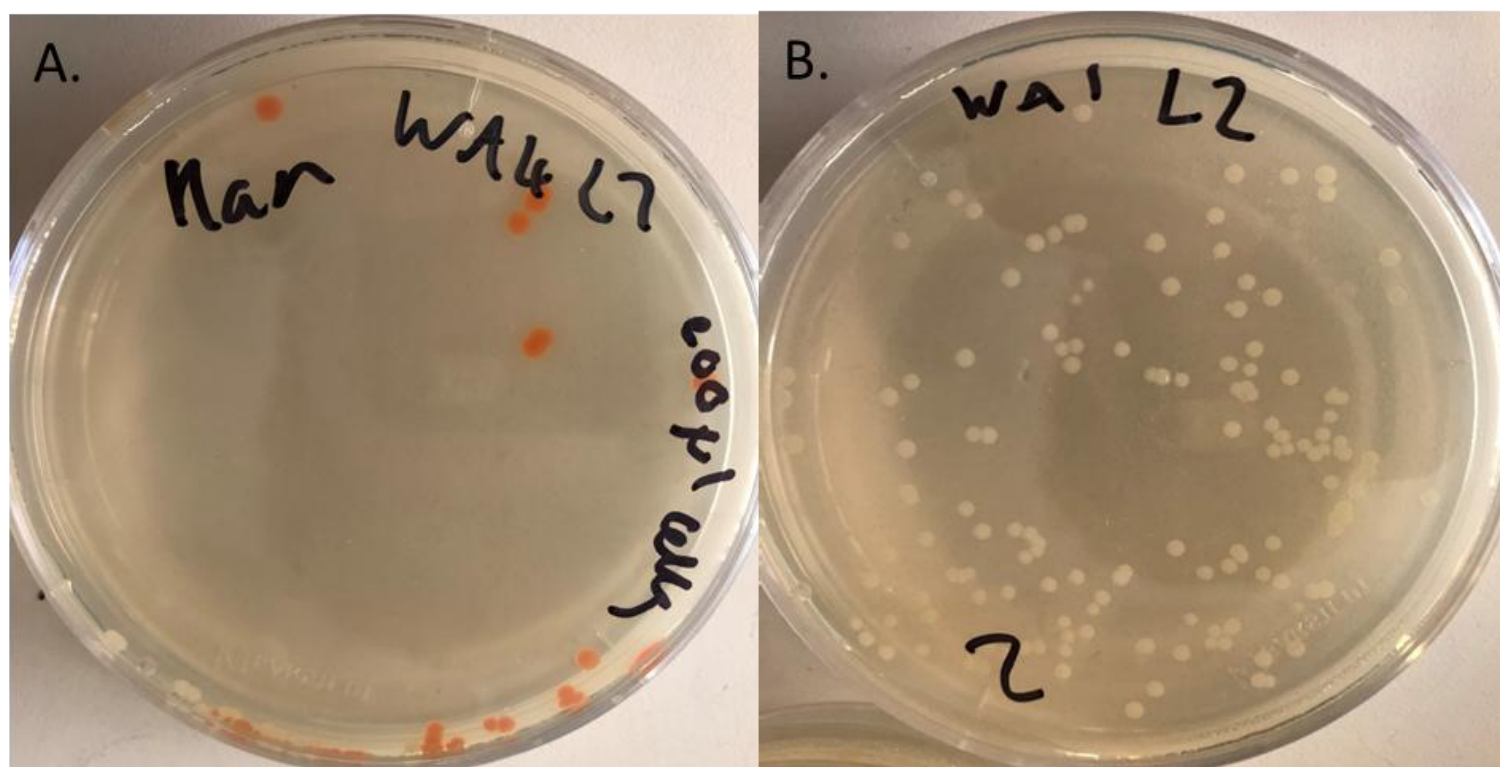
Figure 2.4. Red/white selection of transformed E. coli cells containing a Level 2 Golden Gate final vector. Red colonies contain only the Level 2 destination vector. White colonies contain the Level 2 destination vector with the inserted Level 1 modules.

Plasmids were then prepared for sequencing, accompanied by the primers outlined in Figures 2.5-2.8. Primers were designed so that the junctions between the different components (Level 0 modules) in the Level 1 modules and between the Level 1 modules themselves are sequenced.

Level 2 construct sequences were verified via sequencing using the primers indicated in purple in Figures 2.5-2.8. Correctly assembled Level 2 plasmids were taken forward for plant transformation. Primers for plasmid construct sequencing were designed using the NCBI Primer-Blast tool (NIH, USA), using the designed plasmid sequence as the template.

Name	Query	Direction	Sequence
STO F1	Stomagen	Forward	tagttcaagcctcaagacctcg
HXK F1	Hexokinase	Forward	acggatgcagagctcagggaagtgg
HXK F2	Hexokinase	Forward	ataccgttggaacactagccggtgg
HXK F3	Hexokinase	Forward	atcggttatagccatggatggtgg
Kan vF1	Kanamyicn	Forward	aagatggattgcacgcaggttctcc
Kan vR1	Kanamyicn	Reverse	aacgctatgtcctgatagcggtcc
AHA F1	AHA2	Forward	caagtggagcgaacaagagg
AHA F2	AHA2	Forward	agacaaaggagtccccaggt
AHA F3	AHA2	Forward	gcagatcatggagttttgttga
L0-F(0015)	Level 0 Vector	Forward	cgttatcccctgattctgtggataac
L0-R(K)	Level 0 Vector	Reverse	tcgtatgttgtgtggaattgtgagc
L1M-R-RP	Level 1 Vector	Reverse	gtactggggtggatgcagtg
L1M-R-FP	Level 1 Vector	Forward	cggataaaccttttcacgccc
L2-F	Level 2 Vector	Forward	tggcacatacaaatggacgaacgg
L2-R	Level 2 Vector	Reverse	atgggctgcctgtatcgagtgg
L1-R-KAN1	Level 1 Module (60)	Forward	aactgttcgccaggctcaagg

Table 2.1. PCR Primers used for construct verification during plasmid cloning.

The desired Level 1 module encoding the overexpression cassette of the gene/s of interest (Figure 2.1) and the kanamycin resistance Level 1 module (60) as a selectable marker (Figures 2.5 and 2.6). Constructs shown in Figure 2.1A and D were assembled to form construct 60(WA1) as shown in Figure 2.5. Constructs in Figure 2.1B and D were combined to form construct 60(WA2) as shown in Figure 2.6.
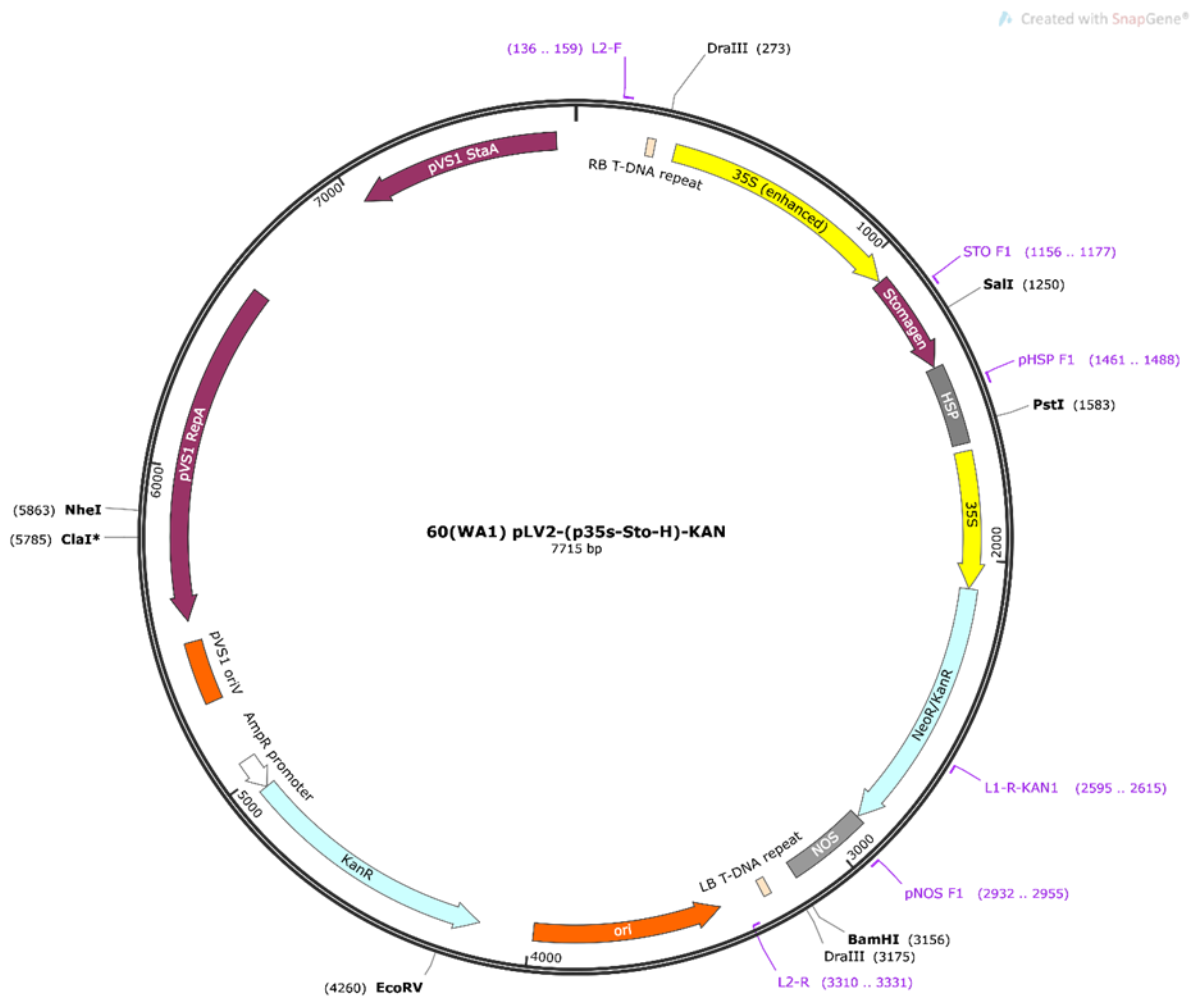
Figure 2.5. The plasmid map of the final Level 2 construct 60(WA1), assembled from constructs A and D in Fig. 2.1. The construct assembly was verified via sequencing using primers indicated by the purple labels. This construct is primarily comprised of the STOMAGEN overexpression cassette and kanamycin resistance. The DNA situated between the Right border (RB) and Left border (LB) T-DNA repeat will be randomly inserted into the plant genome.

Figure 2.6. The plasmid map of the final Level 2 construct 60(WA2), assembled from constructs B and D in Fig. 2.1. The construct assembly was verified via sequencing using primers indicated by the purple labels. This construct is primarily comprised of Guard cell-specific overexpression of Hexokinase and kanamycin resistance. The DNA situated between the Right border (RB) and Left border (LB) T-DNA repeat will be randomly inserted into the plant genome.

Multigene constructs (Figures 2.7-2.8) were assembled using the Level 1 modules shown in Figure 2.1. Level 2 construct 60(WA1-6) (Figure 2.6) is comprised of the combination of Level 1 modules for STOMAGEN overexpression (Fig. 2.1A), Guard cell-specific Hexokinase overexpression (Fig. 2.1B) with kanamycin resistance (Fig. 2.1D).

Figure 2.7. The plasmid map of the final Level 2 construct 60(WA1-6), assembled from constructs A, B and D in Fig. 2.1. The construct assembly was verified via sequencing using primers indicated by the purple labels. This construct is primarily comprised of STOMAGEN overexpression cassette, Guard cell-specific overexpression of Hexokinase and kanamycin resistance. The DNA situated between the Right border (RB) and Left border (LB) T-DNA repeat will be randomly inserted into the plant genome.

3.2. Plant material and growth conditions

3.2.1. Fragaria x ananassa

Strawberry plant material was provided as *in vitro* stock cultures by Niab (Niab, UK). *In-vitro* shoot cultures of *F. x ananassa* 'Calypso' were maintained in a growth room at 21 °C with a 16/8 h light/ dark photoperiod, provided by fluorescent lamps (colour reference 835, colour temperature 3500K). Crowns were subcultured at 4-week intervals, 5-7 per honey jar containing 50 mL medium. Basal culture medium was Murashige and Skoog (MS) macro and microelements and vitamins (Murashige and Skoog, 1962) (4.4 g L^{-1}), supplemented with sucrose (30 g L^{-1}), 6-benzylaminopurine (BAP) 0.1 mg L^{-1} and indole-3-butyric acid (IBA) 0.1 mg L^{-1}, as described by Schaart (2014) (Schaart, 2014). The medium was solidified with Daishin agar (Duchefa D1004, 9 g L^{-1}). The pH was adjusted to 5.8 before autoclaving.

Figure 2.8. In vitro culture of untransformed Fragaria x ananassa 'Calypso' on strawberry propagation media.

Post regeneration, Strawberry plants were hardened by transfer to a vermiculite medium (Dupre Minerals, Staffordshire, UK) with very high humidity in six-cell propagation chambers

(Artcome Ltd., UK). Plants were grown in these conditions for four weeks, with the humidity gradually decreasing by opening the lid vents and then removing the lid, allowing them to acclimate to the external environment.

Figure 2.9. Regenerated strawberry plants undergoing the hardening process in high high-humidity environment growing in vermiculite mineral substrate.

Strawberry plants were then transferred to soil (Levington F2, Fisons, Ipswich, UK). Plants were grown under two distinct environments: Controlled environment (CT Room) and Glasshouse conditions. The CT Room had a temperature of 23°C during the day and 18°C at night, with a relative humidity of 65% and illumination of 300 µmol photons m^{-2} s^{-1}. The Glasshouse environment was the same as the high-light environment outlined, but the experiment ran during the summer, meaning that the daytime temperature ranged from 25-60 °C due to GM containment preventing ventilation.

Figure 2.10. Hardened strawberries growing in a controlled environment (day/night temperature 23/ 18 °C, 65% relative humidity and illumination of 300 µmol photons m^{-2} s^{-1}).

3.3. Strawberry transformation

3.3.1. Transformation of Agrobacterium tumefaciens

A. tumefaciens strain EHA105 (Hood *et al.*, 1993), stored in 25% glycerol, was thawed on ice. The plasmid of interest (Figures 2.5-2.7) was added to thawed bacteria (1 µL, 100 ng mL^{-1}). The tube was flash-frozen in liquid nitrogen for 5 minutes and flash-thawed in a water bath at 37 °C for 5 minutes. The bacterial mix was added to low salt LB broth (700 µL) and shaken at 28 °C for 2 hours. Cells were pelleted by centrifugation at 8000 g for 2 minutes, 600 µL of the low salt LB broth was decanted and discarded, and cells were re-suspended in the remaining 100 µL of media. Cells were plated on low salt agar plates with rifampicin (100 µg mL^{-1}) and the selectable marker (kanamycin 50 µg mL^{-1}) and left to grow at 28 °C for a minimum of 48 hours.

Figure 2.11. Successfully transformed A. tumefaciens strain EHA105.

3.3.2. Transformation of the octoploid strawberry

Transformation of *F. x ananassa* 'Calypso' was performed following (Schaart, 2014), with minor amendments. *Agrobacterium tumefaciens* strain EHA105 (Hood *et al.*, 1993) harbouring the binary vector was grown overnight in a shaker at 28 °C and 180 rpm as a preculture in low salt LB broth with markers (10 mL, rifampicin 100 µg mL^{-1}, kanamycin 50 µg mL^{-1} and streptomycin 50 µg mL^{-1}). The preculture was then added to 80 mL of low salt LB broth, with the same selectable markers and concentrations as the preculture, and was grown overnight in a shaker at 28 °C and

180 rpm. The culture was pelleted at 2,000 g for 10 minutes. An MS-based medium (4.4 g L^{-1}) supplemented with glucose (30 g L^{-1}) and acetosyringone (100 µM) was prepared, pH adjusted to 5.2, and filter sterilised. The bacterial pellet was re-suspended in this medium to give an OD 600 nm 0.2 – 0.3.

Young expanding leaves of *F.* x *ananassa* 'Calypso' were harvested from shoots four weeks after subculture and submerged in the inoculum for approximately 10-15 minutes. Leaflets were separated from each leaf before scoring transversely, leaving one leaf edge intact. Explants were transferred to a filter paper on strawberry regeneration medium (SRM), adaxial face down. SRM is comprised of Murashige and Skoog (MS) macro and microelements and vitamins (Murashige and Skoog, 1962) (4.4 g L^{-1}), supplemented with 1-Naphthaleneacetic acid (NAA) 0.2 mg L^{-1}, thidiazuron (TDZ) 1 mg L^{-1} and filter sterilised glucose (300 g L^{-1}). The medium was solidified with Agargel (Sigma, 5 g L^{-1}) and the pH was adjusted to 5.8 before autoclaving.
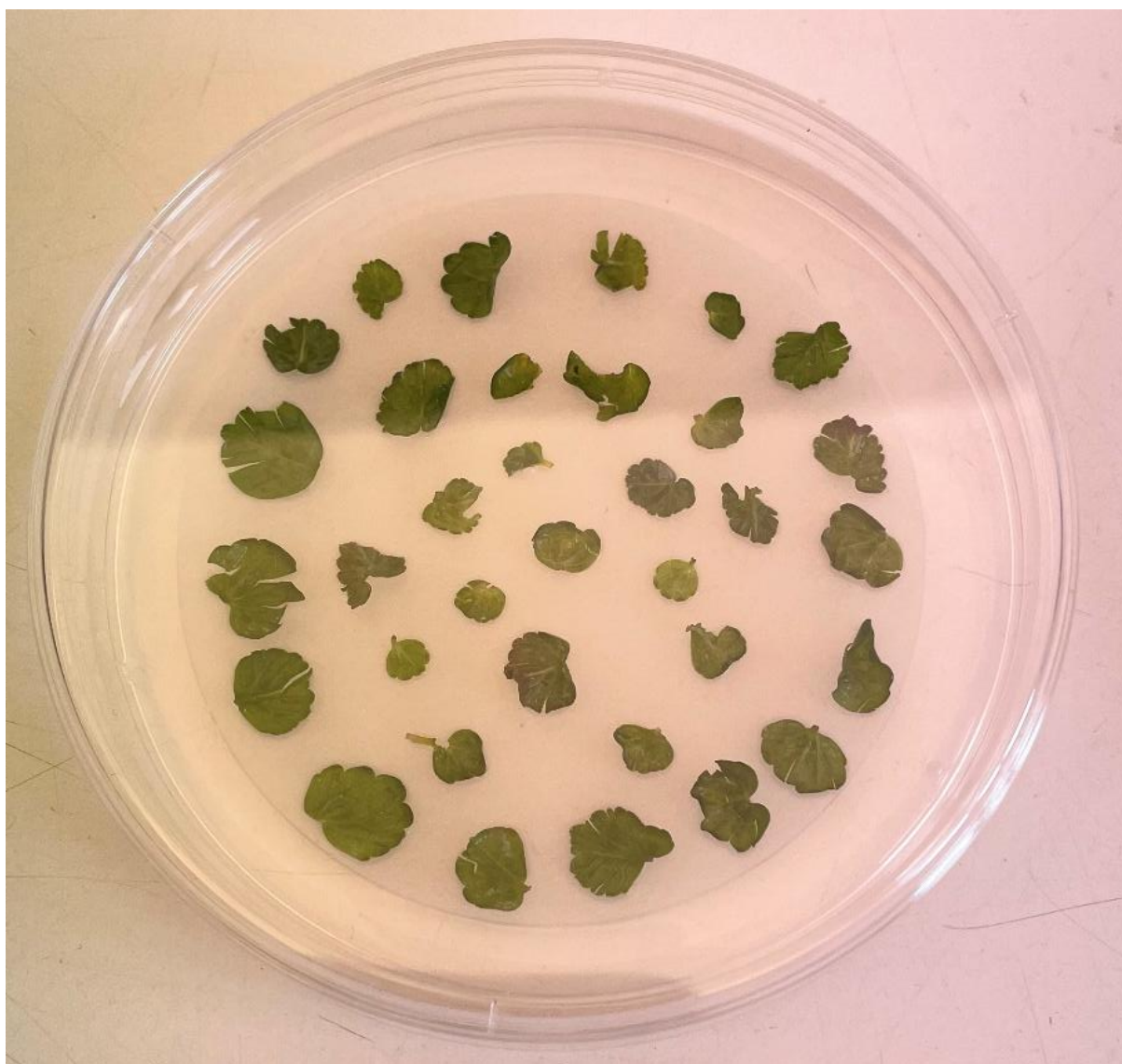
Figure 2.12. Strawberry leaf explants collected from untransformed material were infected with Agrobacterium. Explants are stored in the dark for 4 days on regeneration media without selectable markers. Explants are then subcultured onto regeneration media containing ticarcillin disodium/clavulanate potassium (TCA) for selection against Agrobacterium and kanamycin for selection for transformed tissue.

After four days of dark incubation at 21 °C, explants were transferred to SRM with selectable markers ticarcillin disodium/clavulanate potassium (Duchefa T0190) (400 µg mL^{-1}) and kanamycin (50 µg mL^{-1}). Sterilised filter paper was used to prevent direct contact between the explants and the media. Dishes were sealed with Parafilm® M and incubated in the growth room under the same conditions previously described. Explants were subcultured every 10 days. Leaves were divided between additional dishes as expansion occurred to separate regenerating calli.

Figure 2.13. Excised calli from transformed strawberry leaf explants. Shoot formation can be seen on the central callus.

Callus formation and shoot emergence were seen at approximately 2 months post-infection (Figure 2.14). Regenerating calli were excised and spread over additional plates to allow space for expansion. Emerging shoots were then transferred to the rooting medium once large enough.

Regenerating shoots were transferred to rooting media (FragR) once greater than approximately 2 mm in size and displaying at least 1-2 leaves. FragR is comprised of Murashige and Skoog (MS) macro and microelements and vitamins (Murashige and Skoog, 1962) (2.2 g L^{-1}), supplemented with sucrose (20 g L^{-1}), 6-benzylaminopurine (BAP) 0.1 mg L^{-1} and indole-3-butyric acid (IBA) 0.1 mg L^{-1}. The medium was solidified with Daishin agar (Duchefa D1004, 9 g L^{-1}). The pH was adjusted to 5.8 before autoclaving. Post autoclaving, the medium was additionally

supplemented with ticarcillin disodium/clavulanate potassium (Duchefa T0190) (400 µg mL^{-1}) and kanamycin (50 µg mL^{-1}).

Figure 2.14. A regenerated shoot of 60(WA1) in rooting media (FragR). Small roots have begun to emerge from the shoot and through the remaining callus underneath.

Plants with large root systems were then transferred to strawberry multiplication media (SMM) for crown expansion. SMM FragR is comprised of Murashige and Skoog (MS) macro and microelements and vitamins (Murashige and Skoog, 1962) (4.4 g L^{-1}), supplemented with sucrose

(30 g L^{-1}), 6-benzylaminopurine (BAP) 0.5 mg L^{-1}. The medium was solidified with Daishin agar (Duchefa D1004, 9 g L^{-1}). The pH was adjusted to 5.8 before autoclaving. Post autoclaving, the media was additionally supplemented with ticarcillin disodium/clavulanate potassium (Duchefa T0190) (400 µg mL^{-1}) and kanamycin (50 µg mL^{-1}) to select for putative transgenic plants only.

Roots typically begin to emerge after approximately 2 weeks on rooting media but with a highly variable rate of emergence and development. Once a large root system had been established, then plants were transferred to multiplication media for crown expansion to create an *in-vitro* stock of that event (Figure 2.16). Upon transfer from FragR to SMM, leaf samples were taken for DNA extraction.

Figure 2.15. A regenerated plant of 60(WA2) in SMM for crown expansion. A large root system has developed (not visible).

3.4. Confirmation of transgene insertion

3.4.1. Leaf DNA extraction

Single strawberry leaves were taken from regenerated plants during the transfer from FragR to SMM. Leaf samples were stored in 1.5 mL Eppendorf tubes and frozen in liquid nitrogen for 5 minutes. DNA extraction buffer, comprised of 10% sodium dodecyl sulfate (SDS), 1 M Tris-HCl (pH 8), 0.5 M ethylenediaminetetraacetic acid (EDTA) and polyvinylpyrrolidone (PVP) (0.5 g L^{-1}), was heated to 65 °C pre-extraction. One Qiagen tungsten carbide bead (Qiagen, Manchester, UK) was placed into each sample tube, which was subsequently placed in a Geno/Grinder 2010 (SPEX SamplePrep, Cambridge, UK), which ran at 1500 rpm for 1.5 minutes. 250 μL of preheated extraction buffer was added to each sample, which was then vortexed for 3 seconds. Samples were placed in a water bath at 65 °C for 30 mins, with samples being vortexed every 5 mins. Samples were then centrifuged for 1 min at 4000 rpm. Samples were cooled at -20 °C for 15 minutes before 250 μL of chilled (4 °C) 5 M NaCl was added to each sample. Samples were mixed and incubated at -20 °C for 15 mins. Samples were centrifuged at 4000 rpm for 20 mins, followed by the transfer of the supernatant to 1.5 mL Eppendorf tubes containing 200 μL of isopropanol, which were mixed and stored at -20 °C overnight for DNA precipitation. After overnight storage, samples were centrifuged at 4000 rpm for 20 minutes, and the supernatant was poured out. The pellet was washed by the addition of 500 μL of 70% ethanol and centrifuged at 4000 rpm for 20 mins, then the supernatant was poured away, with all steps being repeated once. The DNA pellet was air-dried for 4 hours, then rehydrated with 125 μL 1 mM Tris-HCl (pH 8). The quality of the extracted DNA was assessed using a Nanodrop 1000 (ThermoFisher Scientific, US) the following day.

3.4.2. PCR verification of transgene insertion

PCR reactions using forward (KanF1-aagatggattgcacgcaggttctcc) and reverse (KanR1-aacgctatgtcctgatagcggtcc) primers for the kanamycin resistance gene present in all Level 2 constructs were done to confirm transgene insertion. The reagents per reaction were as follows: 12.5 µL Quick-Load® Taq® 2X Master mix (New England Biolabs, Hertfordshire, UK), 0.5 µL 10 µM KanF1, 0.5 µL 10 µM KanR1, 1 µL DNA sample and 10.5 µL dH$_2$O. The PCR reaction was as follows: 1x(96 °C for 2 mins), 35x(96 °C for 15 secs, 60 °C for 15 secs, 72 °C for 90 secs) and 1x(72 °C for 5 mins). PCR products were run on a 1% agarose gel for 30 minutes at 145 volts. The banding patterns were compared to the 1 Kb ladder to assess the size, with an expected banding pattern of 657 bp for positive results. The level 1 vector encoding the kanamycin resistance gene and DNA extracted from leaf tissue of untransformed strawberry Calypso stock for their respective reactions were used as the positive and negative controls, respectively.

3.5.   Analysis of transgene expression

3.5.1.   Plant leaf RNA extraction

Leaf samples (100 mg) were harvested from growth conditions, in 1.5µl Eppendorf tubes and immediately frozen in liquid nitrogen. The leaves were then ground using a pestle and mortar in liquid nitrogen to prevent the rapid degradation of the RNA. RNA was extracted using the Nucleospin RNA Plant and Fungi Kit (Macherey-Nagel) according to the manufacturer's instructions. A DNase treatment was applied to the extracted RNA to minimise DNA contamination (Nucleospin rDNase kit, Macherey-Nagel). Concentration and quality of extracted RNA were determined using a Nanodrop 1000 spectrophotometer (Thermo Scientific) to confirm sufficient purity for cDNA synthesis.

3.5.2.   cDNA generation

cDNA was generated using the UltraScript™ 2.0 cDNA Synthesis Kit (PCR Biosystems) according to the kit instructions. RNA samples of various concentrations were diluted to 100 ng µL^{-1}. In each instance, 15 µL of RNA was processed (1500 ng total RNA).

3.5.3. qPCR analysis of transgene expression

Primers for qPCR were designed using NCBI Primer-Blast for *Arabidopsis thaliana*, and *Fragaria x ananassa. (Duch)*. The *A. thaliana* sequence was derived from plasmid sequences for the transgenes. *F x ananassa* sequences were derived from the *Fragaria x ananassa* Camarosa Genome v1.0.a2 (Liu *et al.*, 2021).

F x ananassa specific housekeeping gene primers were taken from Lin et al., 2021(Lin *et al.*, 2021). The guard cell-specific primers for *Fragaria x ananassa* were designed based on the gene sequence for the strawberry homologue of AKT1, based on protein BLAST (maker-Fvb1-4-augustus-gene-10.65-mRNA-1). Primer sequences were as follows:

Gene	Orientation	Sequence	Role
Stomagen	Forward	AGTTCAAGCCTCAAGACCTCG	Transgene
Stomagen	Reverse	GGGTCATTTCCTTCGACTGG	Transgene
HXK	Forward	cgatccctaaatggcatggtctg	Transgene
HXK	Reverse	gaatccaggcgaacagattcttgag	Transgene
26srRNA	Forward	ACCGTTGATTCGCACAATTGGTCATCG	*F.x ananassa* housekeeping gene
26srRNA	Reverse	TACTGCGGGTCGGCAAACGGGCG	*F.x ananassa* housekeeping gene
AHA2	Forward	TGCCGAGTCGCCTTCCAGTT	Transgene
AHA2	Reverse	TTCGACCCACCAAGGCACGA	Transgene
AKT1	Forward	TTTGCAATGGCGTTCAGTGG	*F.x ananassa* Guard cell-specific housekeeping gene
AKT1	Reverse	AGAGAGGGCAGTATTCCGGT	*F.x ananassa* Guard cell-specific housekeeping gene

Table 2.2. qPCR primers

Primers were diluted to 10 µmol. A master mix using the 2x qPCRBIO SyGreen Mix Lo-ROX (PCR Biosystems) was made as follows for a total reaction volume of 20 µL:

Reagent	Volume (µL)
2x qPCRBIO SyGreen Mix	10
Forward Primer	0.8
Reverse Primer	0.8
cDNA	1
dH2O	6.9

Table 2.3. PCR reaction recipe for qPCR.

Samples were pipetted into a white rectangular 96-well plate (ThermoFisher Scientific) covered with transparent plastic (ThermoFisher Scientific). Plates were loaded into the CFX Opus 96 Real-Time PCR System (Bio-Rad) for analysis. Each reaction contained three technical replicates and three biological replicates per cDNA sample (WT reaction included on every plate), three control reactions (no template cDNA) and three null controls (water only). The qPCR programme was as follows:

Cycles	Temperature
1x	95 °C for 10 minutes
40x	95 °C for 15 s followed by 60 °C for 25 seconds

Relative expression levels of the transgene were calculated using the 2(-Delta C(T)) method (Livak and Schmittgen, 2001). Briefly:

1. ΔCt was calculated as the difference between the Ct value of the target gene and the reference gene (House Keeping gene):

$$\Delta Ct = Ct_{Target} - Ct_{Reference}$$

2. Fold change in expression was calculated as:

$$Relative\ expression = 2^{-\Delta Ct}$$

Results were expressed as fold change relative to the reference gene.

3.6.   Phenotypic analysis of transgenic plants

3.6.1.   Microscopy of leaf epidermal peels

Leaf epidermal peels were produced by applying a thin layer of nail polish directly to the abaxial and adaxial leaf surfaces of a recently harvested leaf. Once dried, clear tape was used to gently remove the nail polish, which was then adhered to a microscope slide (ThermoFisher Scientific, US).

Microscopy analysis of epidermal peels was done using a Swift Imaging 5MP camera and its associated SWIFT imaging software (SWIFT, US) attached to a Leica ATC 2000 light microscope (Leica Microsystems, Germany) using 20x magnification for Strawberry. Stomatal density was calculated by counting the total number of guard cells within a defined area (0.18104843 mm). Counts were done on eight unique proximal areas on the epidermal peel. SD counts were first adjusted to 1 mm by dividing by the surveyed area (0.18104843 mm). Adjusted SD values were then averaged to give the SD of that replicate, with a total of 3 biological replicates per line.

Stomatal clustering was measured in plants overexpressing STOMAGEN. Plants with a stomatal clustering phenotype were counted twice: 1. Each guard cell was counted as unique, and 2. Guard cells within a cluster act as a group and thus count as one. The number of clustered stomata was calculated as follows:

$$\text{SD}_{\text{(Clustered stomata)}} = \text{SD}_{\text{(Unique stomata)}} - \text{SD}_{\text{(Clustered stomata act as one)}}.$$

3.6.2.   Gas exchange measurements

Leaf CO2 was measured on the youngest fully expanded leaves using portable open gas exchange systems incorporating CO2 and water vapour infra-red gas analysers (LI-6800, LI-COR Biosciences, Lincoln, NE, USA). Plants were subject to three gas exchange programmes: A/C_i, A/Q and Step-change, the specifics of which are as follows.

1. *A/Cᵢ* Response Curves:

The response of net CO_2 assimilation rate (A) to intercellular CO_2 concentration (C_i) was measured using a portable open gas exchange system (LI-6800, LI-COR Biosciences, Lincoln, NE, USA) equipped with a 6 cm² fluorometer chamber (LI-6800-01A). Measurements were performed on the youngest fully expanded leaves under saturating irradiance (1500 µmol m^{-2} s^{-1} PPFD) supplied by the integrated red/blue LED light source. Chamber conditions were maintained at 25 °C leaf temperature and 65% relative humidity. Flow rate was set to 500 µmol s^{-1}, and reference CO_2 concentration (C_a) was initially held at 400 µmol mol^{-1} until steady-state gas exchange was achieved.

Following equilibration, C_a was decreased stepwise to 250, 150, 100, and 50 µmol mol^{-1}, then returned to 400 µmol mol^{-1} before being increased to 550, 700, 900, 1100, 1300, and 1500 µmol mol^{-1}. At each step, *A* was allowed to stabilise before recording (minimum wait of 90 seconds and maximum wait of 300 seconds).

The maximum carboxylation rate of Rubisco (V_{cmax}) and the maximum electron transport rate supporting RuBP regeneration (J_{max}) were estimated from the *A/Cᵢ* response curves using the Farquhar-von Caemmerer-Berry model (von Caemmerer and Farquhar, 1981) as implemented in the plantecophys package in R (Duursma, 2015). The maximum rate of CO_2 assimilation (A_{max}) was taken as the rate at 1500 µmol mol^{-1} CO_2 under saturating light.

2. Light-response (*A/Q)* Response Curves:

Photosynthetic light-response curves were measured using a portable open gas exchange system (LI-6800, LI-COR Biosciences, Lincoln, NE, USA) fitted with a 6 cm² fluorometer chamber (LI-6800-01A). Measurements were made on the youngest fully expanded leaves under ambient

CO_2 concentration (~400 µmol mol^{-1}) supplied by the reference channel. Chamber conditions were maintained at 25 °C leaf temperature and 65% relative humidity. Flow rate was set to 500 µmol s^{-1}.

Actinic light intensity was applied in the following sequence (µmol m^{-2} s^{-1} PPFD): 1500, 1300, 1100, 900, 700, 550, 400, 250, 100, 0. At each step, leaves were allowed to reach steady-state photosynthesis before data were recorded.

Light-response parameters were estimated by fitting the non-rectangular hyperbola model:

$$A = \frac{\alpha Q + A_{sat} - \sqrt[2]{(\alpha Q + A_{sat})^2 - 4\alpha Q \theta A_{sat}}}{2\theta} - R_d$$

Where A is the net CO_2 assimilation rate (µmol m^{-2} s^{-1}), Q is the incident photon flux density (µmol m^{-2} s^{-1}), α is the apparent quantum yield, A_{sat} is the light-saturated assimilation rate, θ is the curvature factor, and R_d is the dark respiration rate.

Model fitting was performed in R using nonlinear least squares regression, and parameter estimates for A_{sat}, α, and R_d were derived directly from the fitted model.

3. Step-change measurements and modelling of stomatal kinetics

Stomatal conductance (g_{sw}) and net CO_2 assimilation (A) responses to step changes in photosynthetic photon flux density (PPFD) were measured using a portable open gas exchange system (LI-6800, LI-COR Biosciences, Lincoln, NE, USA) with an integrated LED light source (LI-6800-01A). The youngest fully expanded leaf was clamped in the chamber (6 cm²) and equilibrated at low light (50 or 100 µmol m^{-2} s^{-1} PPFD), 400 µmol mol^{-1} CO_2, 25 °C, and a vapour pressure deficit of 1.0 ± 0.2 kPa until steady state was reached. A single rapid increase in PPFD to 1000 µmol m^{-2} s^{-1} was applied, followed by a return to low light (50 or 100 µmol m^{-2} s^{-1})to characterise stomatal opening and closing kinetics, respectively.

Step-change program was as follows:

- 100 µmol m^{-2} s^{-1} for 900 s, 1000 µmol m^{-2} s^{-1} for 2700 s, then 100 µmol m^{-2} s^{-1} for 1800 s

Strawberry).

Measurements were logged every 10 seconds for all experiments except HXK/AHA T2, which were logged every 3 seconds.

Stomatal kinetics were quantified by fitting separate sigmoidal models to the opening (step-increase) and closing (step-decrease) phases, adapted from Vialet-Chabrand et al. (2017) (Vialet-Chabrand *et al.*, 2017). The step-increase model was:

$$g_{sw}(t) = (G_{max} - G_{min})e^{-e^{\left(\frac{\lambda-t}{k_i}+1\right)}} + G_{min}$$

and the step-decrease model was:

$$g_{sw}(t) = (G_{min} - G_{max})e^{-e^{\left(\frac{\lambda-t}{k_d}+1\right)}} + G_{max}$$

where *t* is time (s), λ is the inflexion point of the response, *k* is a time constant describing the rate of change, and G_{min} and G_{max} are the asymptotic minimum and maximum conductance values, respectively.

All model fitting was conducted in R (version 4.5.1), with parameter estimates extracted for subsequent statistical analysis.

3.7.   Statistical analyses

All statistical analyses were conducted in R (version 4.5.1; R Core Team, 2025) using RStudio (Posit Software, PBC). Data were inspected for normality and homogeneity of variance before hypothesis testing. Where assumptions of normality were met, comparisons between groups were performed using one-way or two-way analysis of variance (ANOVA) followed by Tukey's honestly significant difference (HSD) post-hoc test. Where assumptions were violated, non-parametric equivalents were applied. Model fitting for stomatal kinetics was performed using non-linear least

squares (nls) with separate fits for the step-increase and step-decrease phases. Coefficients of determination (R^2) and 95% confidence intervals were calculated for each fitted model. Data visualisation was performed using the ggplot2 and ggpubr packages, with figures generated directly from processed data to ensure reproducibility. Statistical significance was accepted at $p < 0.05$ unless otherwise stated.

4. Results

4.1. Molecular validation of transgenic lines

4.1.1. PCR confirmation of NPTII insertion in transformed lines

To confirm the insertion of the transgene into the genome of the putative transgenic strawberry line, a PCR was used to confirm the presence of the positive selection marker NPII and thus, by proxy, the presence of the transgene/s (Fig. 3.1). Transformed plants display a band at 658 bp, in concordance with the positive control (Band 2, Figure 3.1). Lines with no bands at the expected position were classified as escapes and thus grouped into an Azygous line. Following the PCR analysis, only plants that exhibited an appropriate band were selected for vegetative stolon propagation and further analysis.
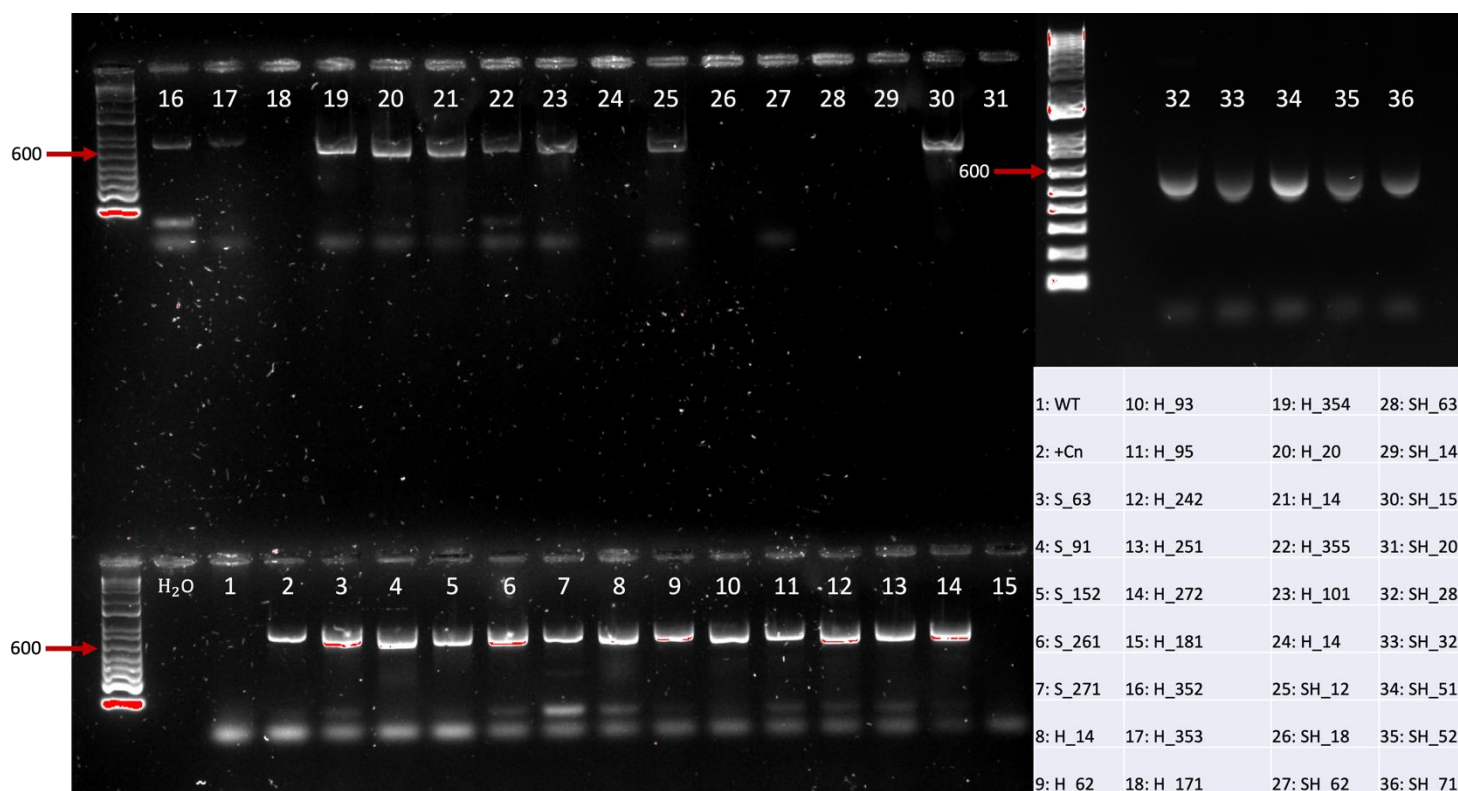
Figure 3.1. Agarose gel showing the banding patterns of DNA fragments produced from a PCR using the forward and reverse primers for the kanamycin resistance gene (NPII) and DNA from putatively transformed strawberry plants. Positive results display a banding pattern of 658 bp. The Level 1 module 60 encoding kanamycin resistance was used as a positive control (+ Cn) and DNA extracted from the untransformed stock of F. x ananassa 'Calypso' was used as a negative control (WT).

4.1.2. Qualitative detection of transgene expression via PCR with cDNA

As a secondary qualitative screen to transgene insertion, PCR analysis of cDNA synthesised from total leaf RNA was used to visualise the expression of both the transgene(s) and resistance gene *NPII* (Figure 3.2). Bands of a size 658 bp indicate a positive reaction and the expression of the resistance gene for kanamycin *NPII* (Figure 3.2A and B), bands of a size 183 bp (Figure 3.2A) and 181 bp (Figure 3.2B) indicate a positive reaction and the transgenic expression of STOMAGEN and Hexokinase, respectively. No bands are observed for the WT negative controls wells 1 upper, lower and well 1(S) *(NPII, Hexokinase and STOMAGEN, respectively)*

*(*Figure 3.2B). Lines with no presence of either resistance gene or transgene expression, later quantitatively confirmed via qPCR (Figure 3.3), were considered Azygous.

### 4.1.3.   Quantitative expression analysis of STOMAGEN and Hexokinase
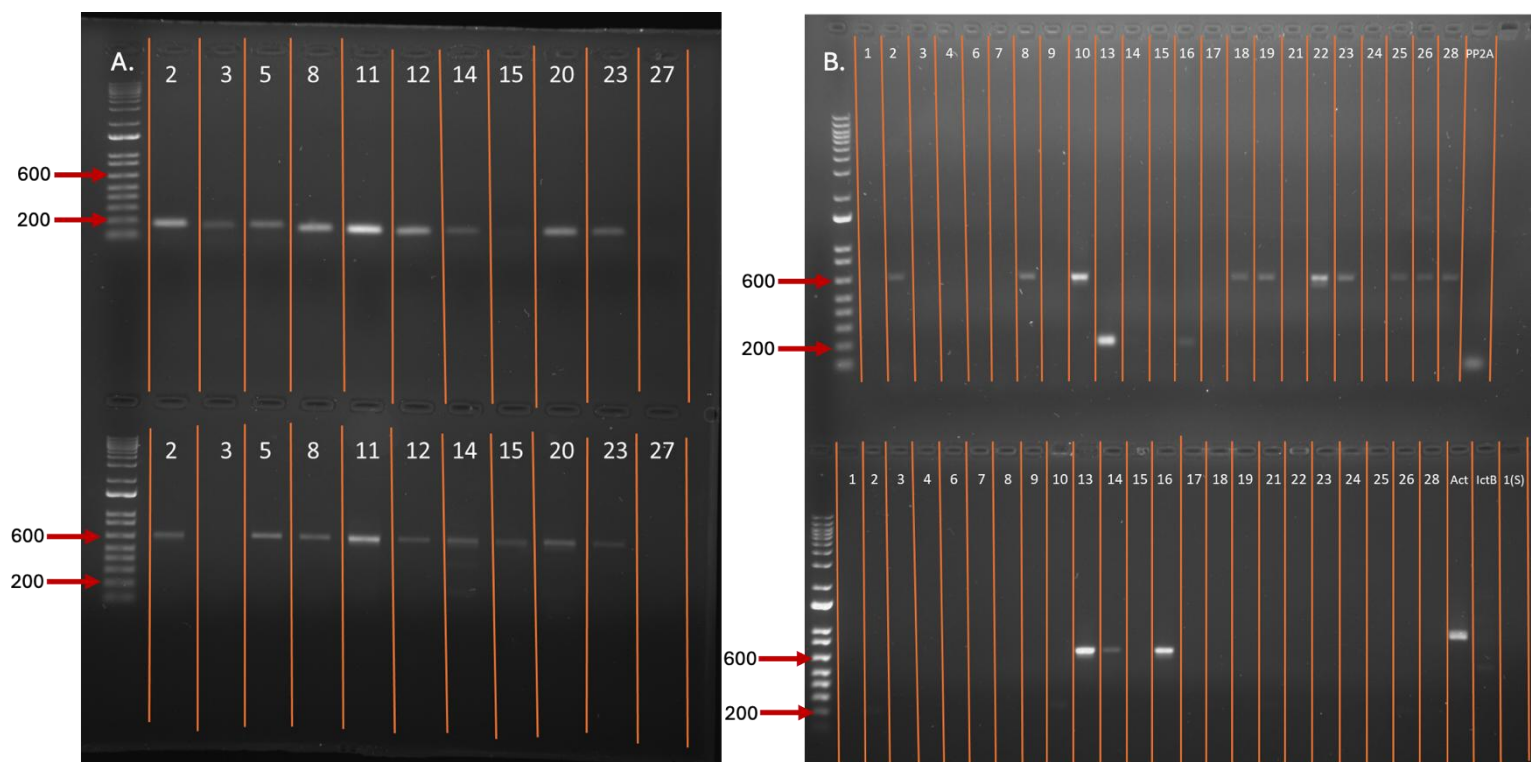
Figure 3.2. Agarose gel shows the banding patterns of DNA fragments produced from a PCR reaction using the forward and reverse primers for Stomagen (A), Hexokinase (B) and the resistance gene for kanamycin NPII on cDNA synthesised from RNA from strawberry leaf samples. Positive results for Kanamycin display a banding pattern of 658 bp (upper band), 183 bp for Stomagen and 181 bp for Hexokinase. The numbers at the top of the wells correspond to the cDNA label of the transgenic line in Table 2.1.

To select transgenic lines of interest, quantitative PCR was used to compare relative transgene expression between lines of interest (Fig. 3.3). Transgenic plants had a wide range of expression levels for STOMAGEN and Hexokinase, relative to 26S rRNA and the strawberry orthologue of the guard-cell-specific ion channel GORK. For STOMAGEN and Hexokinase (Fig. 3.3A and B), statistical group A had little to no detectable expression levels, equivalent to the azygous, and thus were considered azygous. STOMAGEN lines (Fig. 3.3A) formed six distinct expression groups (including the azygous) (ANOVA, Tukey HSD, $p < 0.05$), with a range of

expression from 0.00064 to 0.004x relative to 26S rRNA. Double overexpressing lines, SH_32 and SH_71, had the highest levels of expression (Groups D and E, ANOVA, Tukey HSD, $p < 0.05$). Hexokinase lines fell into five statistical groups (Fig. 3.3B) (ANOVA, Tukey HSD, $p < 0.05$). Hexokinase lines had a range of expression from 0.6 to 6x that of the strawberry orthologue of GORK. One single line, H_354, and two double lines, SH_15 and SH_71, had the highest levels of relative expression (ANOVA, Tukey HSD, $p < 0.05$).
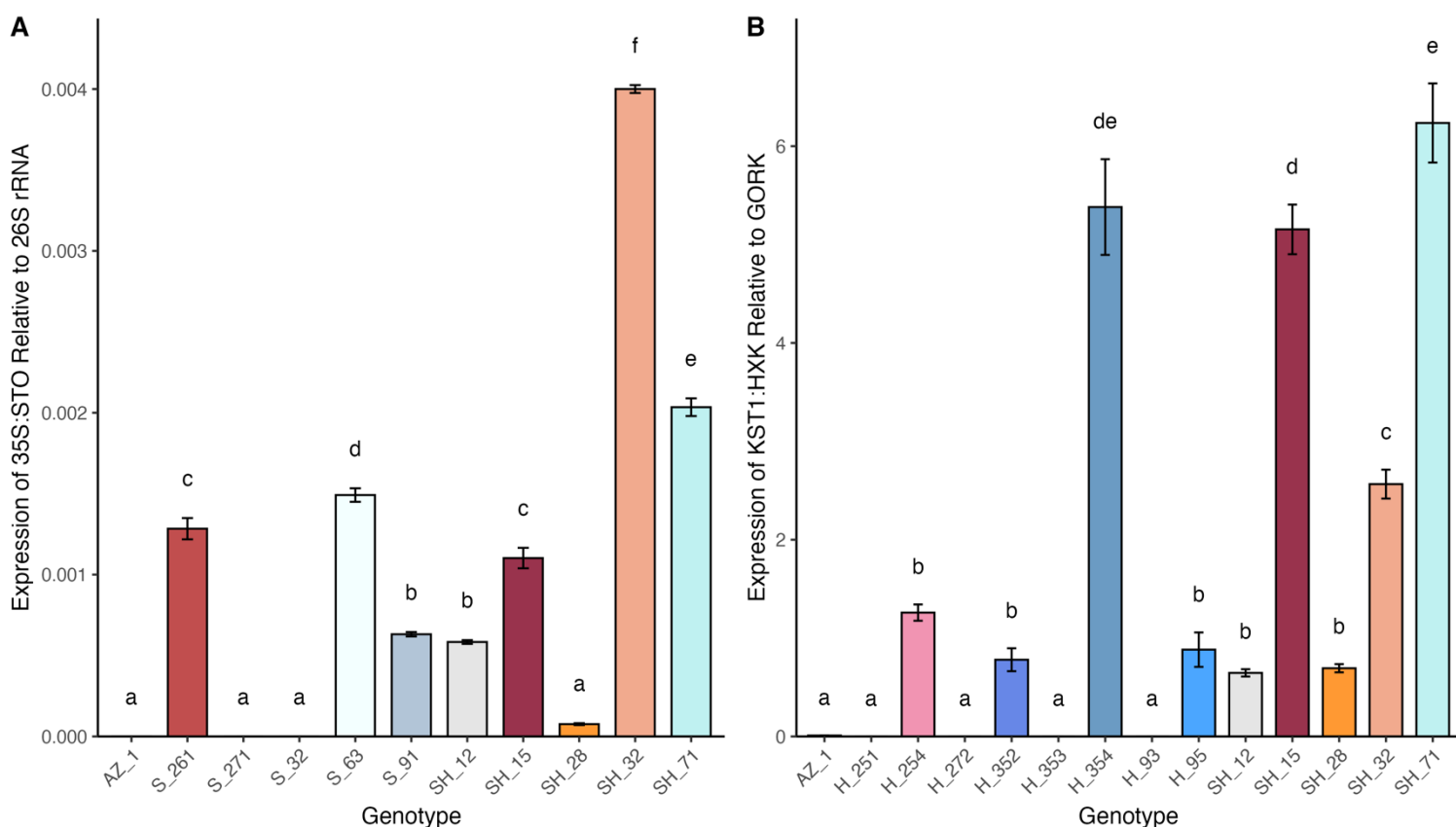
Figure 3.3. Quantitative PCR (qPCR) analysis of relative expression of the transgenes 35S Stomagen and KST1 Hexokinase in transgenic Strawberry lines. Stomagen and Hexokinase were amplified using their respective qPCR primers (Table 1, Chapter 2). STOMAGEN transgene expression was normalised to the expression of 26S rRNA, and Hexokinase was normalised to AKT1 ortholog in Strawberry (Fvb1-4_1088267..1088726 (- strand)). Relative expression of the genes was calculated by normalising expression to the respective WT housekeeping gene.3

4.2. Microscopic characterisation of stomatal development

4.2.1. Changes in epidermal patterning in transgenic lines

To assess the epidermal changes resulting from the overexpression of the transgenes, SD in epidermal peels was quantified using brightfield microscopy. Transgenic strawberry plants overexpressing STOMAGEN not only displayed greater stomatal densities, but also frequent incidences of stomatal clustering (a violation of the one-cell spacing rule) (Fig. 3.4). Stomata formed clusters accounting for 7.2-23.1% of total stomata of all surveyed areas and were present in all surveyed areas of STOMAGEN overexpressing lines. Stomatal clusters ranged from groups

of 2 to 10 (possibly even higher) stomata per cluster. Stomatal clusters were produced in a variety of orientations, but typically, high clusters of higher numbers formed a chain of stomata 'top to tail'. Stomatal clustering occurred seldom in Azygous and Hexokinase overexpressing lines.

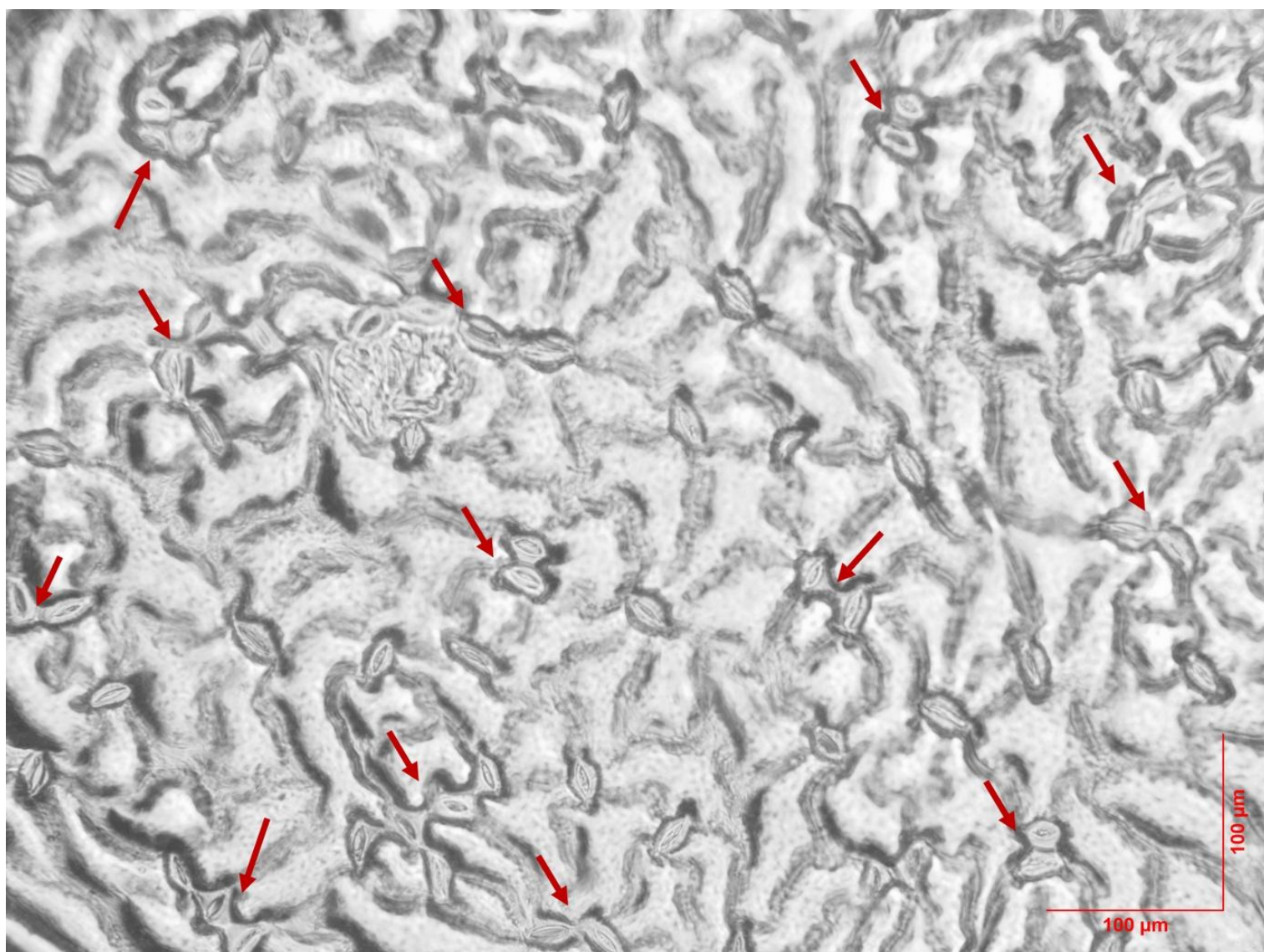*Figure 3.4. Brightfield microscopy images of transgenic strawberry leaf epidermal peels under 20x magnification. The epidermis of this exemplar STOMAGEN overexpressing line shows the stomatal clustering phenotype typically observed in these lines. Stomatal clusters are indicated by the red arrows. These impressions were taken from strawberries grown in a CT Room environment, 23 °C and 65% RH.*

4.2.2.   Quantification of Stomatal Density across transgenic genotypes

The transgenic strawberry lines produced had significantly different stomatal densities when grown in the CT Room environment. Strawberry is a hypostomatous species, having stomata only on the abaxial leaf surface. Azygous lines had an average abaxial SD of 210 (±2.68) stomata mm^{-2}. STOMAGEN overexpressing line S_32 and double lines SH_51 and SH_52 showed no significant difference in abaxial SD (Fig. 3.5, Statistical group A), which reflects the lack of transgene expression for S_32, as outlined in Figure 3.3 (Lines SH_51 and SH_52 were lost to disease before expression analysis was done). STOMAGEN overexpressing lines in statistical groups C, D, E and F had significantly higher SD than the Azygous, with an SD average ranging from 240 to 400 stomata mm^{-2}. Hexokinase lines either showed no significant difference in SD from the Azygous (Statistical group A: H_251, H_352, H_353, H_354, H_93) or significantly reduced SD with an average SD range of 175 to 188 stomata mm^{-2} (Group B: H_14, H_242, H_254, H_62, H_95). All lines were hypostomatous, with stomata only present on the abaxial surface. STOMAGEN overexpressing lines did not have additional stomata present on the adaxial leaf surface. These data suggest that transgenic overexpression of STOMAGEN increases abaxial stomatal density but is unable to induce stomatal development on the astomatous adaxial surface, and that guard-cell-specific hexokinase can decrease stomatal density in ~50% of lines produced.
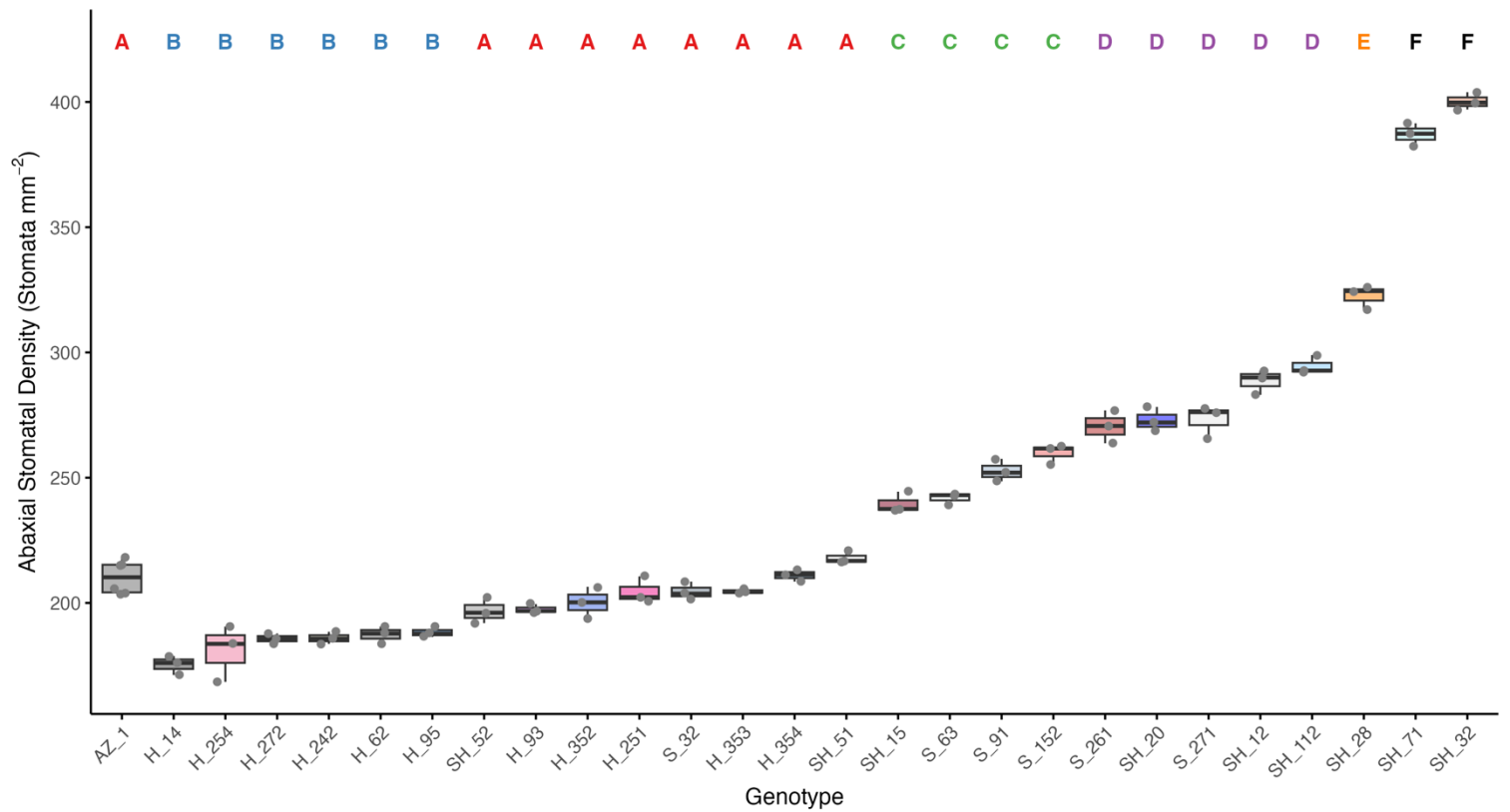
Figure 3.5. Stomatal density comparison between transgenic Strawberry lines grown in the CT room environment (23 °C, 65% RH and 350 mol m^{-2} s^{-1} white light). Stomatal density counts were done on 8 areas of an epidermal peel to form a sample average (n= 3-6). Statistical groupings (CLD) are displayed by the letters above each respective genotype (ANOVA, Tukey test, p < 0.05).

To better understand the effect of transgenic STOMAGEN expression on stomatal density, relative STOMAGEN expression was correlated against SD and clustered SD (number of stomata in clusters mm^{-1}). A strong positive statistically significant correlation was detected between STOMAGEN expression and the number of clustered stomata per mm^2 (R^2 = 0.866, p < 0.001) (Fig. 3.6B), while no significant association was found between 35S::STO expression and total stomatal density (R^2 = 0.416, p = 0.084) (Fig. 3.6A). This data suggests that 35S::STO expression has a strong association with stomatal clustering under these growth conditions, rather than a uniform increase across the epidermis.
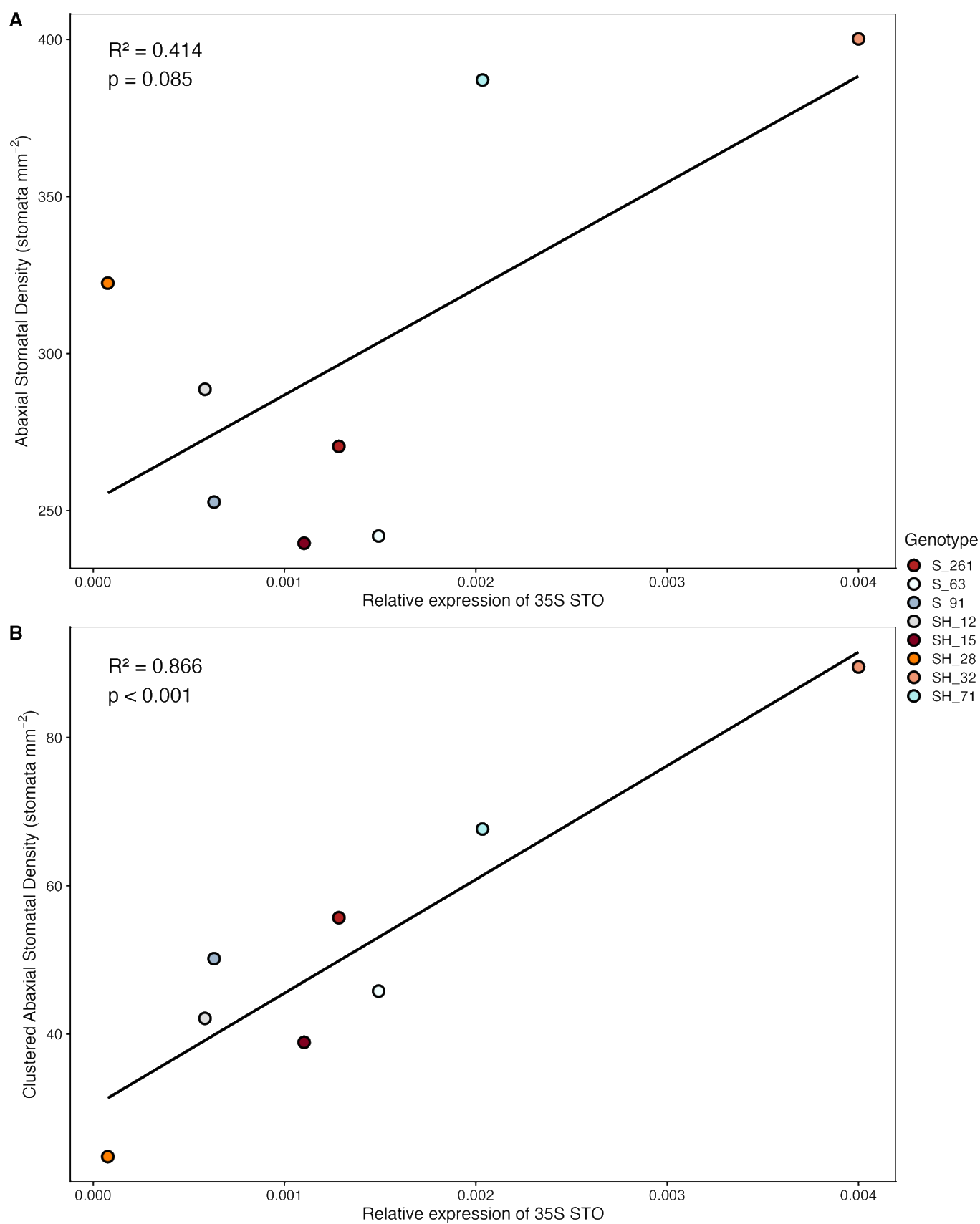
Figure 3.6. Correlation between 35S::STO expression and stomatal patterning traits in transgenic strawberry lines. Each point represents a genotype, coloured by genotype identity. The top panel (A) shows abaxial stomatal density (stomata mm $^{-2}$) plotted against relative 35S::STO expression. The bottom panel (B) shows abaxial clustered stomatal density (clustered stomata mm $^{-2}$) for the same genotypes. Linear regression lines are shown in black, with associated coefficients of determination (R^2) and p-values reported in each panel.

4.2.3. Comparison of Stomatal Patterning Across Growth Environments

To assess how extreme greenhouse temperatures influenced epidermal development, additional stomatal patterning measurements were collected from transgenic strawberry plants grown under these conditions (Fig. 3.7). No statistically significant differences in abaxial SD were detected between genotypes ($p > 0.05$). While visual differences in median stomatal density were observed, for example, higher values in S_71 and lower values in H_95 (313 and 232 stomata mm^{-2}, respectively), these differences were not statistically significant. These findings suggest that, within the surviving genotypes, stomatal density is similar across all transgenic lines and is not significantly influenced by the transgenes under the tested conditions, contrary to what was previously observed on the same plants grown under the CT Room conditions (Fig. 3.5).
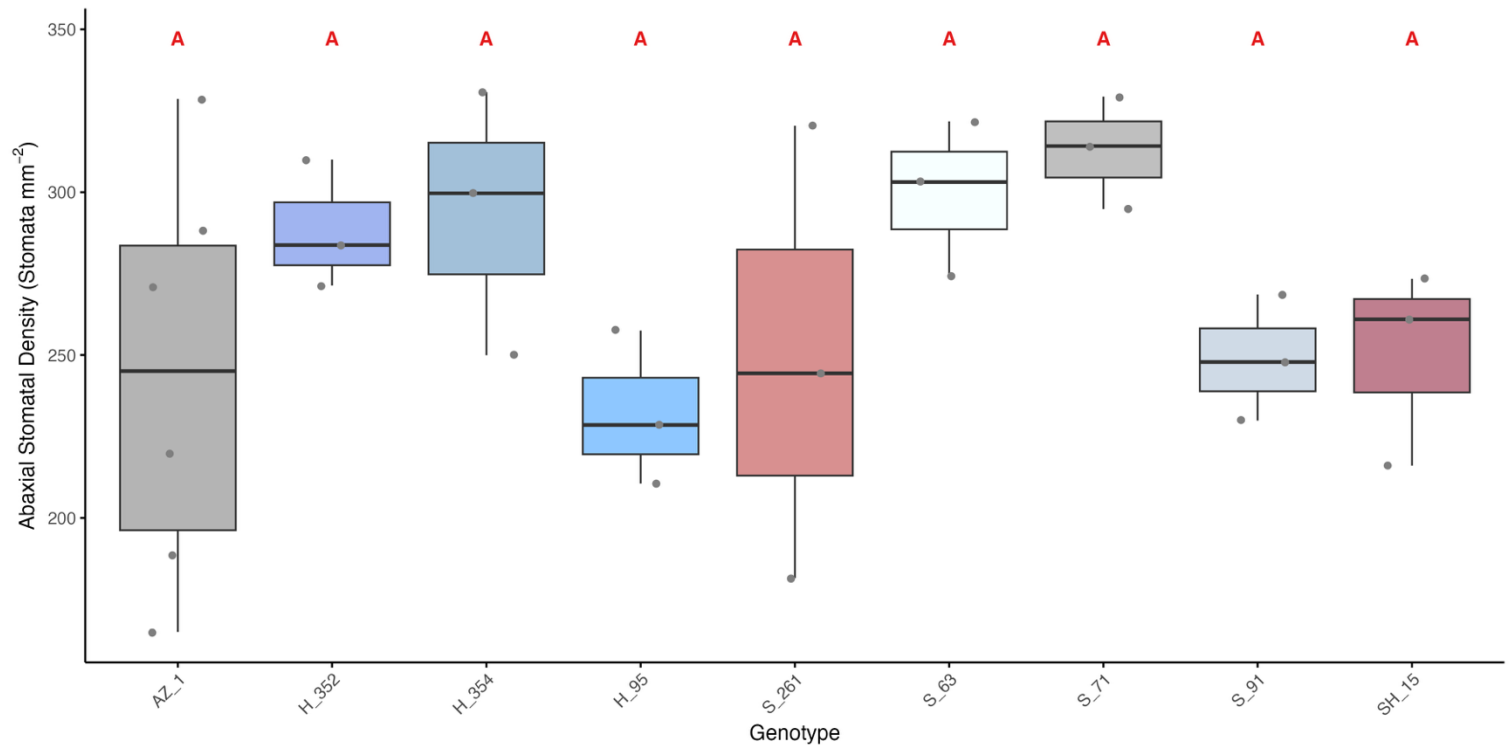
Figure 3.7. Stomatal density (stomata mm⁻²) on the abaxial surface of nine transgenic strawberry genotypes in the Glasshouse environment. Boxplots show the distribution of stomatal density measurements per genotype, with individual data points overlaid. Different shades represent different genotypes. Compact letter display (CLD) annotations above each box indicate statistical groupings based on ANOVA, followed by Tukey's HSD test ($p < 0.05$); genotypes sharing the same letter are not significantly different from one another.

To determine whether the stomatal density of individual lines differed between growth environments, two-sided t-tests were conducted for each genotype, comparing plants grown in the CT Room and the Glasshouse (Fig. 3.8). A significant effect of environment on stomatal density was identified for genotype H_352 ($p = 0.0107$), with higher SD values observed in the glasshouse. Trends toward significance were detected for H_354, S_63, and H_95 ($p = 0.0722$, 0.0515, and 0.0836, respectively), where increased stomatal densities were observed on plants grown under glasshouse conditions. For the remaining genotypes (AZ_1, S_261, S_91, and SH_15), no significant differences were detected in SD irrespective of the growth environments, indicating that the effect of environmental conditions on stomatal development varied among genotypes and the effects of the transgenes on stomatal density were reduced for the same plants grown in a stressful environment.
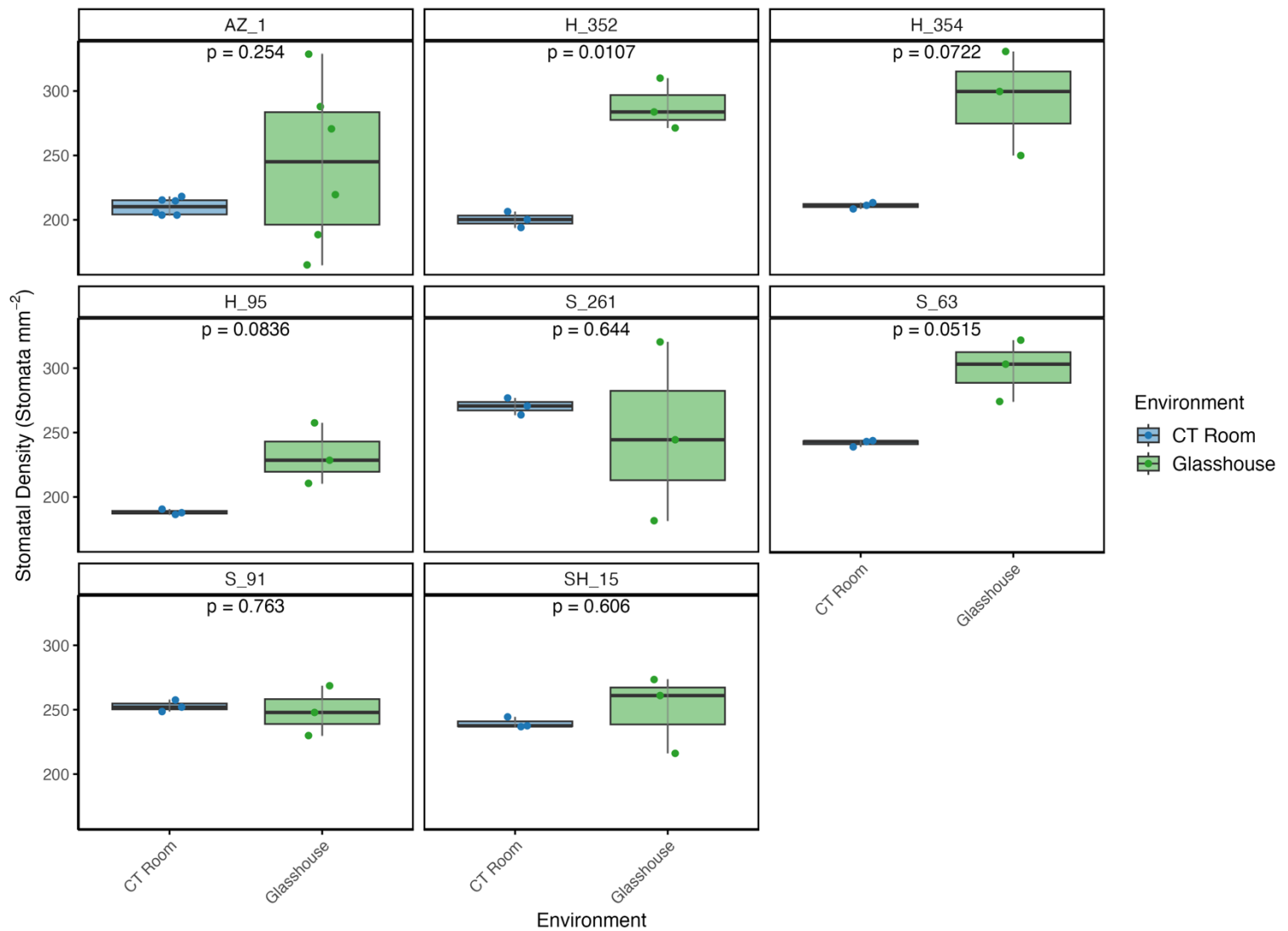
Figure 3.8. Stomatal density (stomata mm $^{-2}$) across two growth environments, CT Room and Glasshouse, for nine transgenic strawberry genotypes. Each panel represents a different genotype, with the genotype displayed as the title for each plot. Boxplots show the distribution of stomatal density per environment, with individual data points overlaid. P values from two-sided t-tests are displayed above each panel, comparing the environments for each genotype. Colours indicate environment: blue for the CT Room and green for the Glasshouse. Environmental conditions per growth environment are as outlined in Methods (Chapter 2.2.2)

4.3. Plant Disease and Management

4.3.1. Disease Symptoms and Plant Survival Under Controlled Conditions

During the course of the project, transgenic strawberry plants were severely affected by pests, diseases, and environmental stress. The first challenge was a Whitefly infestation (Fig. 3.9A). Although this did not kill plants, it necessitated quarantine and intensive pesticide treatments, which prevented measurements at a stage when many lines still had sufficient replicates. The major loss of material occurred later due to widespread Strawberry Crown Rot (Fig. 3.9B), which eliminated numerous unique lines. Surviving plants were then weakened by a severe outbreak of Powdery Mildew (Fig. 3.9C). While this disease caused limited direct mortality, it greatly reduced plant vigour and completely halted stolon production, preventing the generation of new replicates by vegetative propagation. A subsequent infestation of Spider Mites (Fig. 3.9D) added further stress and compounded the overall decline in plant health. Powdery mildew and mite infestations were managed with pesticide applications, soapy water washes, and removal of infected tissue, allowing a few plants to recover. These were transferred from the CT room to glasshouse conditions, where vigorous new growth was observed. However, exposure to high light and temperatures of up to 55 °C in the glasshouse led to further losses (Fig. 3.9E). Altogether, 22 of the 27 transgenic lines were lost, either directly through disease or effectively through a reduction in replicate numbers below three.
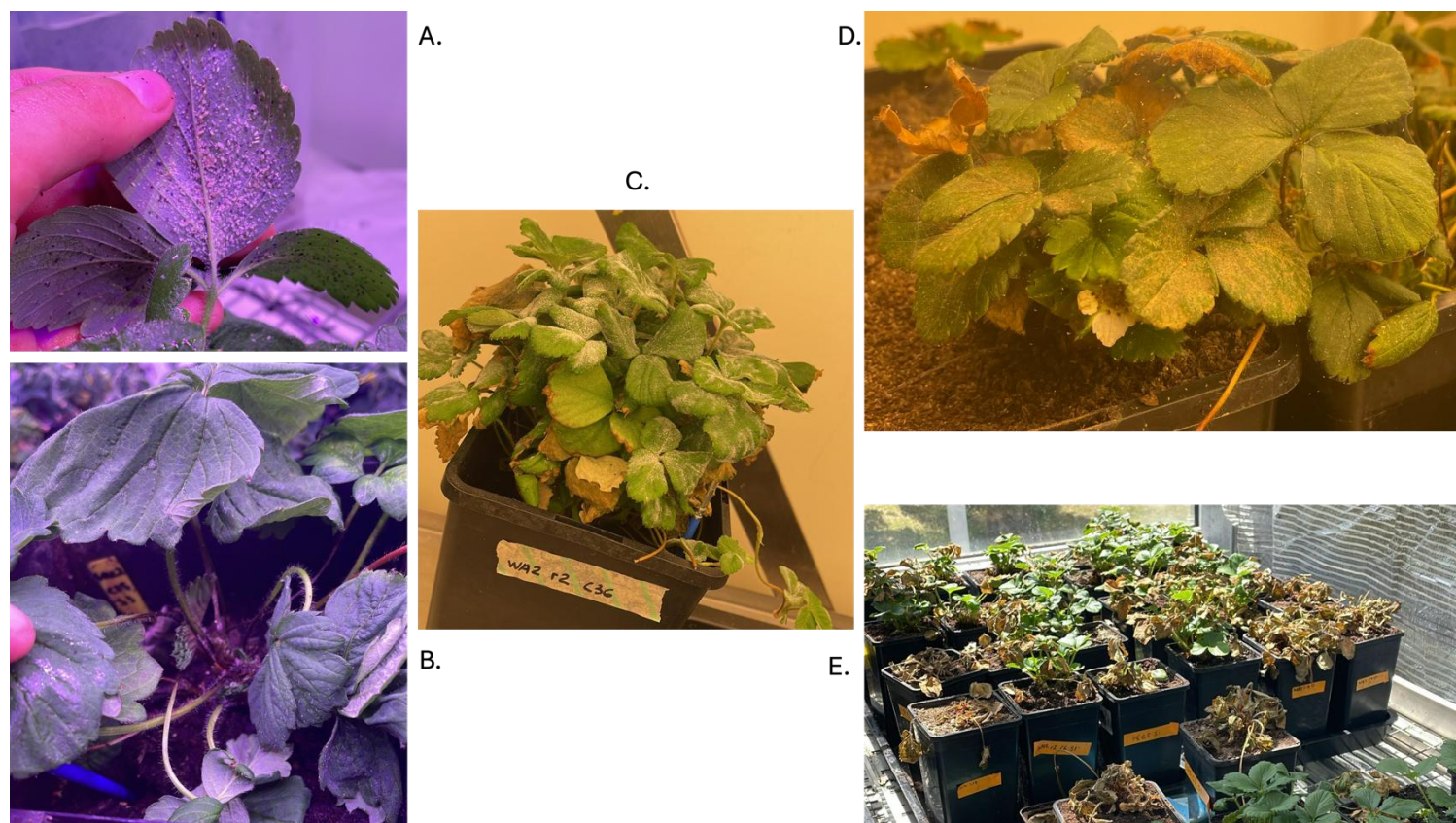
Figure 3.9. Pictures of transgenic strawberry plants afflicted with a variety of plant diseases and stresses throughout experimentation. Plants were afflicted with White fly (Trialeurodes vaporariorum) (A.), water stress/ Crown and Root rot (Phytophthora cactorum, Rhizoctonia spp.) (B.), powdery mildew (Podosphaera aphanis) (C.), Spider mites (family Tetranychidae) (D.) and sun/ heat stress (E.).

4.4. Determining photosynthetic capacity via photosynthetic response to intracellular CO₂ concentrations

4.4.1. A/C_i response curve and genotypic comparison of derived photosynthetic parameters

A/C_i response curves were used to determine if transgenic expression of STOMAGEN and/or Hexokinase affected photosynthetic capacity. All genotypes exhibited a typical *A/C_i* response curve, with the assimilation rate (A) displaying a rapid linear increase at low intercellular CO_2 concentrations (C_i) before plateauing when approaching saturation at higher C_i levels (Fig. 3.10).
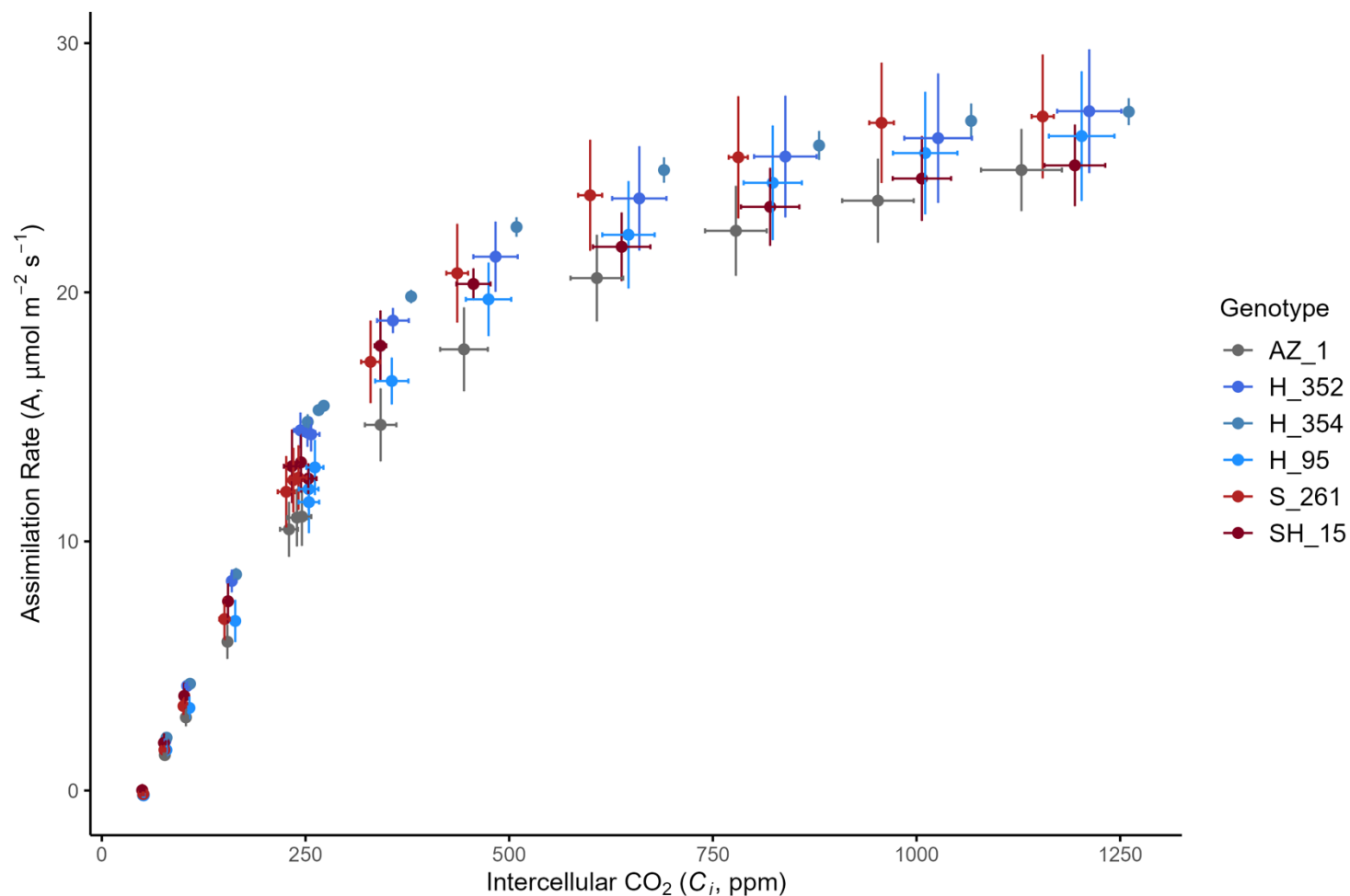
Figure 3.10. Photosynthetic response of transgenic strawberry plants under different intracellular CO2 concentrations (C_i). The net CO_2 assimilation rate (A, $\mu mol\ m^{-2}\ s^{-1}$) is plotted as a function of intercellular CO_2 concentration (C_i, $\mu mol\ mol^{-1}$). Each point represents the mean (n = 3, n = 5 for AZ_1) for a given genotype, with the error bars indicating standard error (SE), for A and C_i (vertical and horizontal, respectively).

While some genotypes, such as H_352 and H_354, tended to exhibit higher A values at elevated C_i, these trends were not statistically supported by modelled photosynthetic parameters (Fig. 3.11). Derived values of A_{max}, Vc_{max}, and J_{max} did not differ significantly between genotypes (ANOVA, Tukey's test, $p < 0.05$), suggesting that the transgenic expression of STOMAGEN and/or Hexokinase did not affect the maximum rate of photosynthesis, maximum rate of carboxylation, or the maximum rate of electron transport.
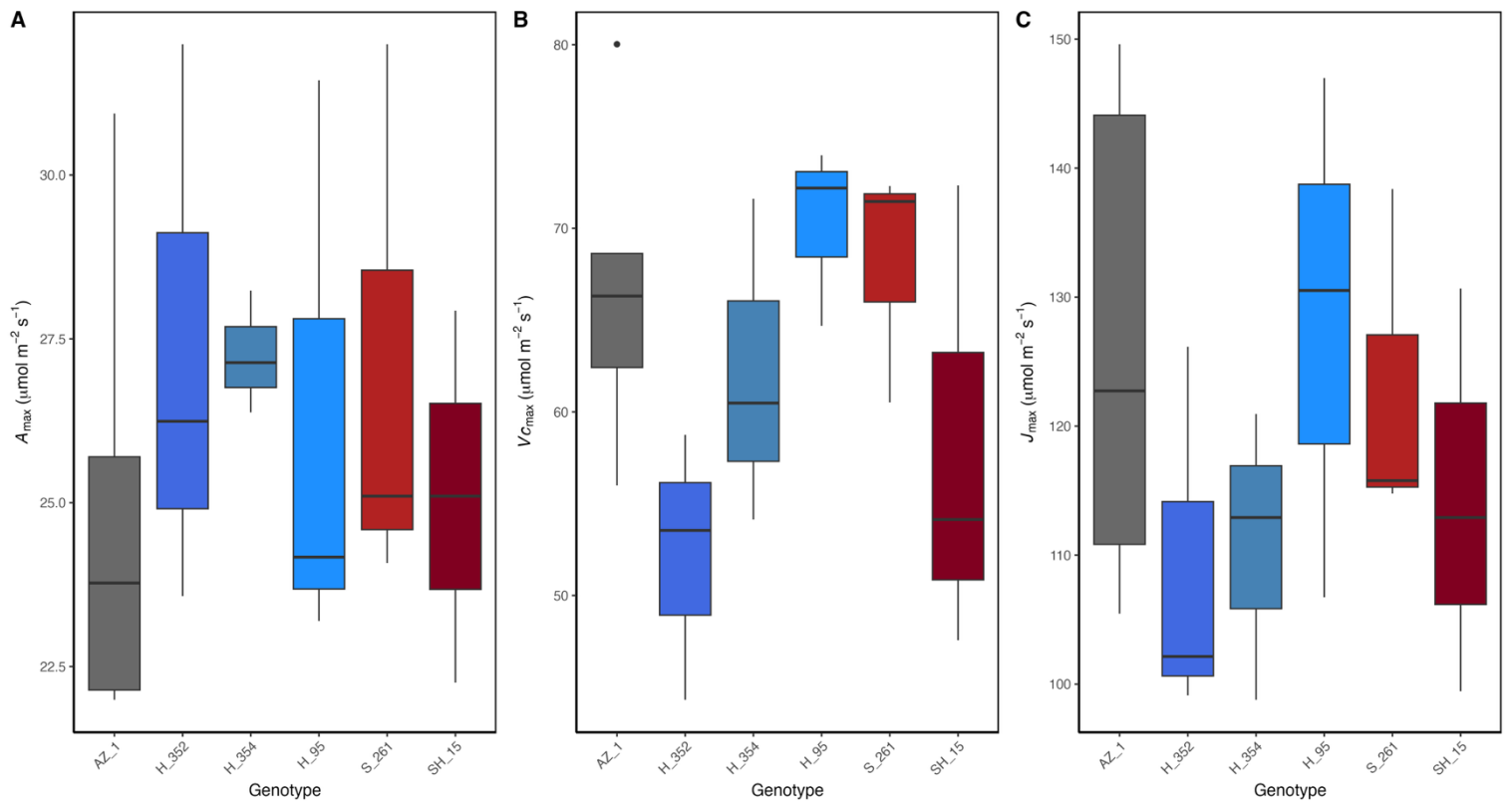
Figure 3.11. Photosynthetic parameters modelled from A/C$_i$ curves across genotypes. (A) CO₂ and Light-saturated assimilation rate (A$_{max}$), (B) maximum Rubisco carboxylation capacity (Vc$_{max}$) and (C) maximum electron-transport rate (J$_{max}$). Boxplots display the median (horizontal line), interquartile range (box), and whiskers extending to 1.5 × the interquartile range, with black dots marking observations beyond this range (outliers).

4.4.2. Stomatal conductance, photosynthesis and intrinsic water use efficiency dynamics in response to dynamic light

To assess genotypic differences in stomatal responses to induced opening and closure, transgenic strawberry plants were subjected to step-changes in light intensity. Following a step-increase in light intensity (100 to 1000 μmol m^{-2} s^{-2}), all genotypes exhibited a rapid rise in net photosynthesis (A) and stomatal conductance to water vapour (g_{sw}), with peak values occurring just before the step-decrease in light intensity (Fig. 3.12). After the return to low light (shaded region), both A and g_{sw} declined across genotypes. Intrinsic water-use efficiency ($iWUE$) increased in most genotypes following a step-increase in light intensity, before declining sharply after a step decrease in light intensity.
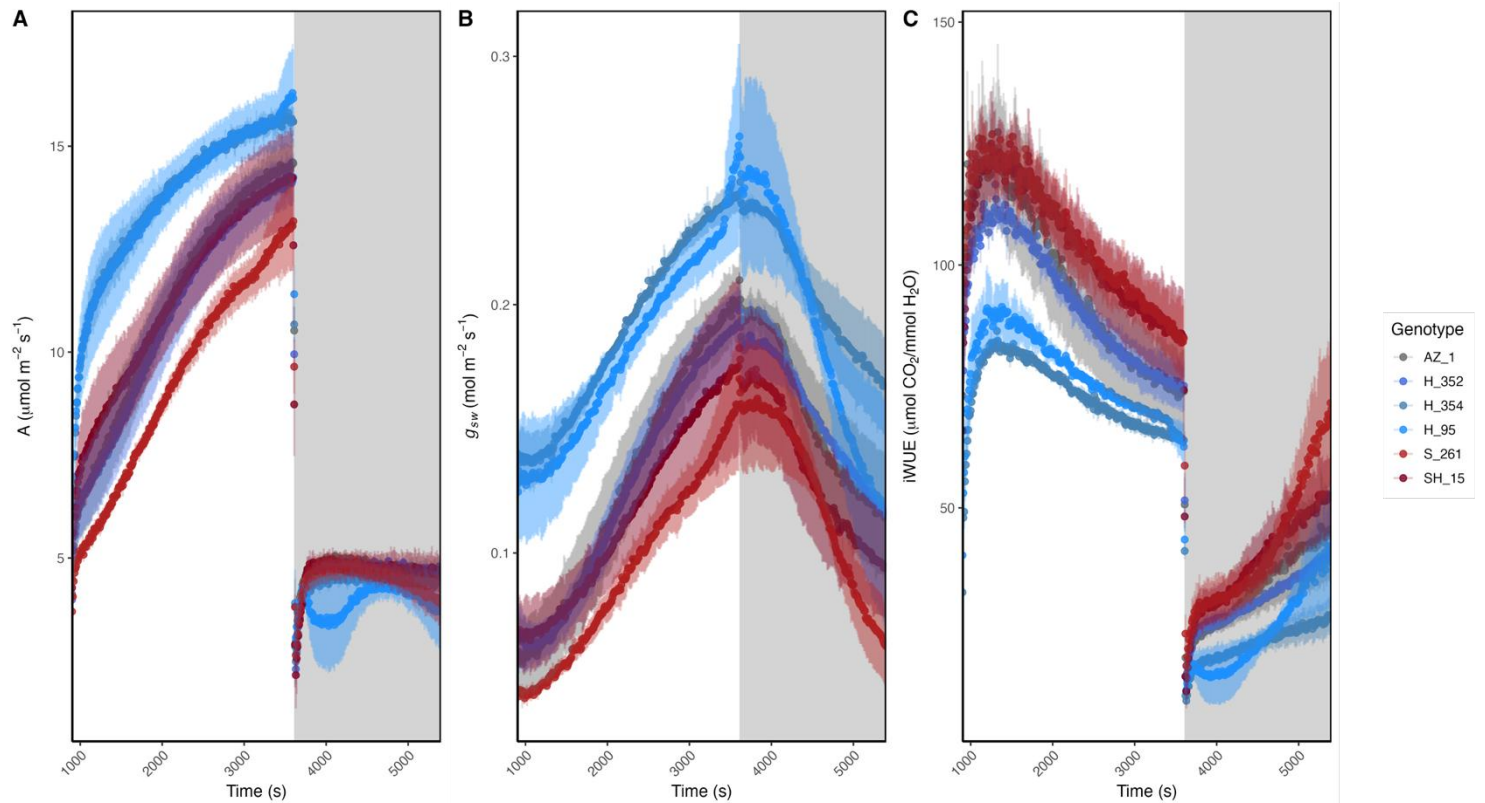
Figure 3.12. Time-course responses of (A) net photosynthesis (A), (B) stomatal conductance to water vapour (g_{sw}), and (C) intrinsic water-use efficiency (iWUE) in transgenic strawberry lines during step changes in light intensity. Light intensity increased from 100 to 1000 µmol m^{-2} s^{-1} at 900 s and returned to 100 µmol m^{-2} s^{-1} at 3600 s, as indicated by the shaded region. Lines represent genotype means; ribbons show ± standard error (n = 8-36).

To determine genotypic differences in the stomatal responses, three distinct time points were chosen to analyse genotypic differences during the step increase and decrease in light intensity: steady-state pre-induction (100 µmol m^{-2} s^{-1}, 900 s), High-Low transition (1000 µmol m^{-2} s^{-1}, 3600 s) and steady-state post-induction (100 µmol m^{-2} s^{-1}, 5400 s). Significant differences were found between genotypes for g_{sw} and iWUE at the steady-state pre-induction time point (100 µmol m^{-2} s^{-1}, 900 s). The hexokinase overexpressing line H_354 had significantly higher g_{sw} than the azygous control, fellow HXK line H_352 and STOMAGEN line S_261 (ANOVA, Tukey HSD, p = 0.025, 0.027 and 0.007, respectively). The HXK line H_95 also trended towards having higher g_{sw} than the azygous control, but was not significant at the 5% threshold (ANOVA, Tukey HSD, p = 0.067); however, this line had significantly higher g_{sw} than the STOMAGEN line S_261 (ANOVA,

Tukey HSD, p = 0.019). The inverse relationship was seen for iWUE, with H_354 having significantly lower iWUE than the azygous control and S_261 (ANOVA, Tukey HSD, p = 0.038 and 0.006, respectively). The HXK line H_95 also had significantly lower iWUE than the STOMAGEN line S_261, but did not differ statistically from the control (ANOVA, Tukey HSD, p = 0.02 and 0.12, respectively). These data suggest that guard-cell-specific overexpression of hexokinase can lead to higher low-light steady-state g_{sw} and, as a result, reduced iWUE.

Normalising A and g_{sw} to the initial and final values of each step change enables visualisation of induction rates and the genotypic differences therein (Fig. 3.13). While apparent genotypic differences can be seen in relative A during the step increase in light intensity (Fig. 3.13A), no statistical differences were found between genotypes for the time taken to reach 33, 50, 66 and 90% of the relative A (ANOVA, Tukey HSD, all p > 0.05). These data suggest that the expression of the transgenes did not alter the rate of photosynthetic induction during a step increase in light intensity.
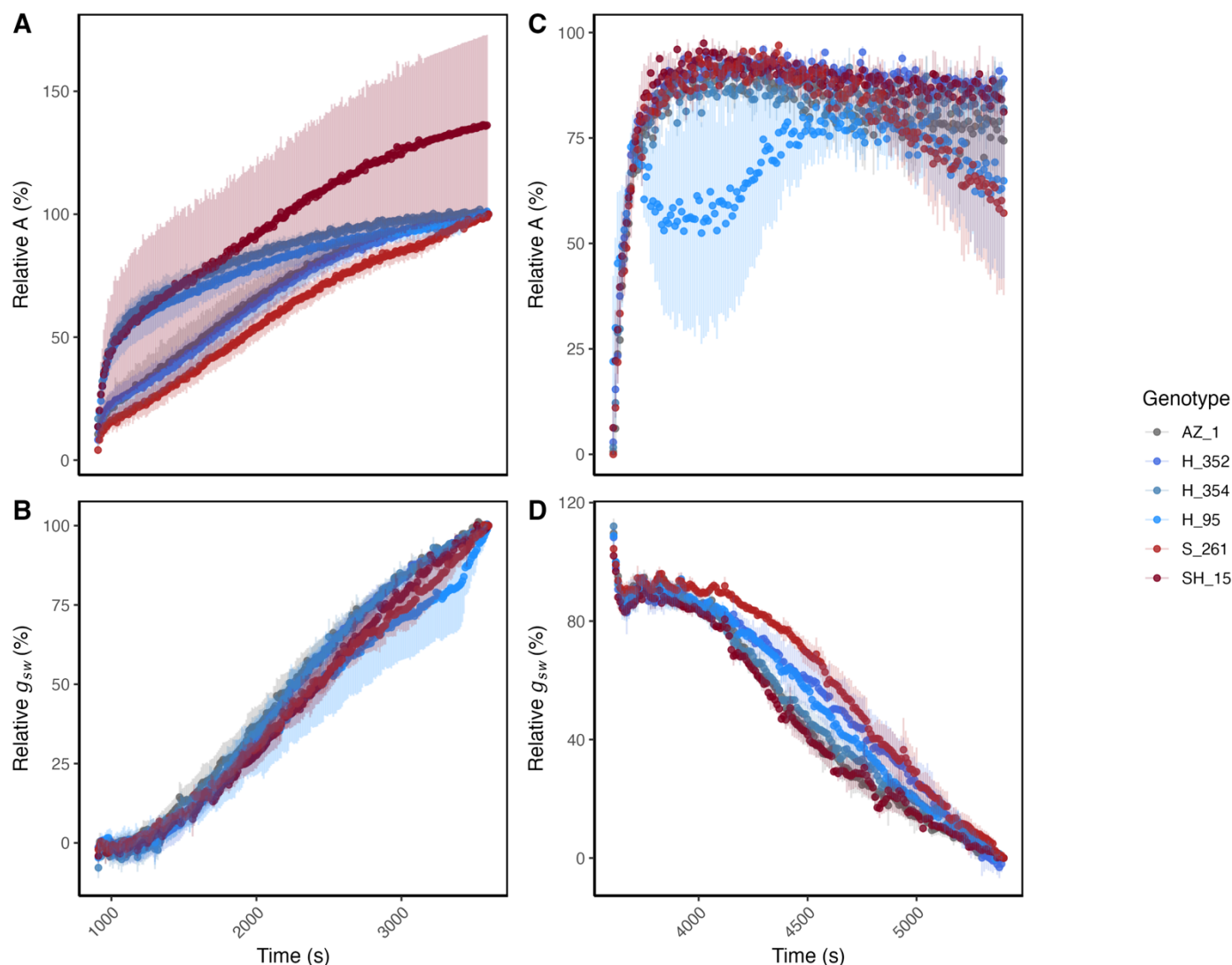
Figure 3.13. Relative CO_2 assimilation (A, %) and stomatal conductance (g_{sw}, %) response to a step change in light intensity over time in transgenic strawberry mutant genotypes. The x-axis represents time (seconds), and the y-axis represents relative A and g_{sw} (%), normalised to initial values (outlined in Chapter 2). The left panels show the response of A (A) and g_{sw} (B) to a step-increase in light intensity, where light intensity increased at Time = 900 s, while the right panel show the response of A (C) and g_{sw} (D) to a step-decrease in light intensity, where light intensity decreased at Time = 3600 s. Each coloured line represents the mean response for a specific genotype, with shaded areas indicating standard error (SE).

To identify if constitutive overexpression of STOMAGEN and/or the guard-cell-specific overexpression of hexokinase altered stomatal behaviour during the step changes in light intensity, stomatal kinetics (k, the time constant describing the speed of stomatal movement) and lag time (l,

time before a significant stomatal response) were modelled according to Vialet-Chabrand et al. (2017) (Vialet-Chabrand *et al.*, 2017). No significant differences were found between genotypes for stomatal kinetics (k) in either the step-increase in light intensity (Kruskal-Wallis, p = 0.5774) or step-decrease in light intensity (ANOVA, p = 0.752), nor for stomatal lag time (l) of the step-increase or decrease in light intensity (ANOVA, p = 0.934 and p = 0.242, respectively) (Fig. 3.14).

When comparing genotypic responses to a step-increase versus step-decrease in light intensity, STOMAGEN overexpressing lines S_261 and SH_15 had a trend towards greater stomatal kinetics in response to a step-increase than to a step-decrease in light intensity (Two Sample t-test, p = 0.062 and p = 0.060, respectively), but no significant differences in stomatal kinetics (k) were found. Significantly lower lag time (l) in response to a step-decrease in light intensity was found for H_354 and SH_15 (Two Sample t-tests, p < 0.01), with no significant differences found for the other genotypes. The other hexokinase overexpressing lines H_352 and H_95 displayed a trend towards a lower stomatal lag time (l) in response to a step-decrease in light intensity (Two Sample t-test, p = 0.064 and p = 0.058), as well as the Azygous (Two Sample t-test, p = 0.083). The trend of having a shorter delay in stomatal response to closure (l in response to a step-decrease in light intensity) in all lines except the STOMAGEN single line S_261 suggest STOMAGEN expression may interfere with an innate rapid response to closure signals. These data suggest that the transgenic expression of hexokinase did not result in any changes in stomatal response to changes in light intensity, but STOMAGEN expression alone may interfere with an apparent innate rapid response to closure signals.
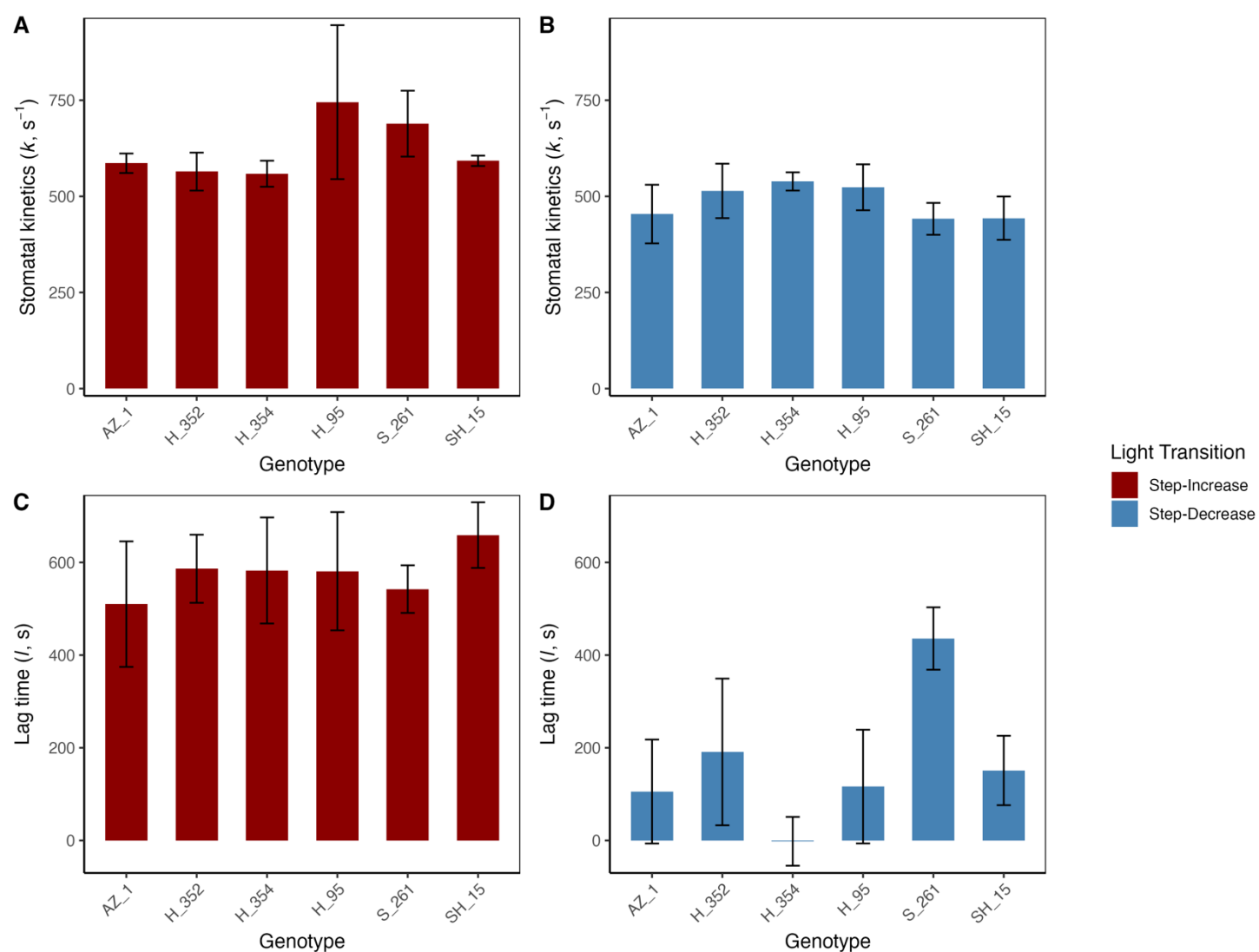
Figure 3.14. Stomatal response kinetics across transgenic strawberry genotypes during light step transitions. (A) Stomatal kinetics parameter (k) and (B) lag time (l) for transgenic strawberry genotypes during a step-increase and step-decrease in light intensity. Bars represent genotype means (± standard error) for each phase, with red bars indicating responses during light induction (Step-Increase) and blue bars during light reduction (Step-Decrease). Stomatal kinetics (k) reflects the rate of the g_{sw} response to a light step change, while lag time (l) represents the temporal delay before the onset of response. Statistical differences are denoted by asterisks and brackets between comparisons (ANOVA with Tukey HSD, * p < 0.05, ** p < 0.01, *** p < 0.001) above the bar charts.

5.   Discussion

Improving stomatal traits has the potential to enhance both photosynthetic performance and water-use efficiency. In particular, manipulating stomatal density (SD) and guard cell function provides complementary routes to influence leaf gas-exchange dynamics. Increased SD will raise the anatomical maximum for stomatal conductance (g_{smax}) and improve CO_2 uptake under high light (Tanaka *et al.*, 2013; Sakoda *et al.*, 2020), while altered guard cell metabolism can directly modify the responsiveness of stomata to environmental and internal signals (Kelly *et al.*, 2013; Lugassi *et al.*, 2015). The cultivated strawberry (*Fragaria × ananassa*) has previously been shown to have a significant stomatal limitation on photosynthetic carbon assimilation, particularly after midday (Yokoyama *et al.*, 2023). Enhancing SD through overexpression of *STOMAGEN* could therefore alleviate these constraints by increasing maximum diffusive capacity, while simultaneous expression of *HXK1* in guard cells offers a strategy to improve water-use efficiency and prevent excessive transpiration, providing a complementary balance between carbon gain and water conservation.

In this study, *STOMAGEN* was constitutively overexpressed to enhance stomatal development, while *HXK1* was expressed specifically in guard cells using the KST1 promoter, to assess their individual and combined effects on gas exchange dynamics and plant productivity. The overexpression of STOMAGEN successfully increased stomatal density but also led to frequent clustering, which appeared to impair function by slowing the lag time to closure in response to environmental signals. By contrast, HXK expression did not alter stomatal kinetics but often increased steady-state g_{sw} under low light. Interestingly, in double transgenic lines, HXK partially rescued the impaired closure response associated with clustering, reducing lag times and restoring more functional stomatal behaviour. Although the experimental timeline was complicated by repeated biotic stresses that reduced overall plant vigour, these results demonstrate that different genetic routes to modify stomatal traits in strawberry have contrasting outcomes: STOMAGEN increases density but compromises function when clustering occurs, whereas HXK may improve

baseline conductance without negatively impacting responsiveness, and can even compensate for defects introduced by clustering.

5.1.1. Effect of transgenes on epidermal patterning

The transgenes overexpressed in strawberry had varying impacts on epidermal patterning (Fig. 3.4-3.5). Under low-stress conditions in the CT room environment, KST1::HXK lines (H) showed stomatal densities consistent with those of the Azygous (AZ) plants or slightly reduced (22-35 stomata mm^{-2} less). Previous work with KST1::HXK tomato and citrus plants also showed no differences in stomatal density between WT and transgenic plants (Kelly *et al.*, 2013; Lugassi *et al.*, 2015). Moreover, since stomatal density is determined during epidermal development, well before the mature guard cells are functional, it seems biologically implausible that expression of HXK *within guard cells* would directly alter the number of stomata (Geisler, Nadeau and Sack, 2000; Nadeau and Sack, 2002; Shpak *et al.*, 2005; Bergmann and Sack, 2007; Hara *et al.*, 2007, 2009; Nadeau, 2009). Therefore, while some of our lines show lower SD, this is more likely to be due to natural line-to-line variation, positional effects of transgene insertion, subtle developmental differences or subtle microclimatic differences, rather than a causal effect of HXK expression (Bhat and Srinivasan, 2002; Casson and Gray, 2008; Casson and Hetherington, 2010; Schnell *et al.*, 2014; Nunes *et al.*, 2022). Differences in environmental conditions, such as water stress, as well as disease stress from Crown and Root rot (*Phytophthora cactorum* and *Rhizoctonia spp*.) and strawberry powdery mildew (*Podosphaera aphanis*), are likely strong contributors to the lowering of SD. These plants may have decreased stomatal density as a defence mechanism to limit pathogen entry, as bacterial infections can systemically suppress SD, resulting in lower SD on leaves developing post-infection (Dutton *et al.*, 2019). Black root rot in strawberries has previously been shown to result in a loss of root function and root mass, which could produce a physiological stress response akin to drought stress (LaMondia, 2004). Leaves developing under severe drought

conditions have shown reduced stomatal development (lower stomatal index (SI) or SD) across multiple species, which may explain the reduction in SD seen in KST1::HXK strawberries, previously unseen in other species (Xu and Zhou, 2008; Hamanishi, Thomas and Campbell, 2012; Ouyang *et al.*, 2017; Mano, Madore and Mickelbart, 2023).

STOMAGEN overexpressing lines (S and SH) had increased SD alongside stomatal clustering. Figure 3.6 illustrates the relationship between the relative expression of 35S::STO and two key stomatal traits: total stomatal density (SD) and the density of clustered stomata. The lack of a significant relationship between 35S::STO expression and SD suggests that while STOMAGEN overexpression may promote stomatal initiation, its effect is modulated by additional regulatory inputs. Stomatal density is influenced by a combination of environmental factors (such as light, humidity, and CO_2 concentration) and endogenous signals, including phytohormones and developmental cues (Lake, Woodward and Quick, 2002; Casson and Hetherington, 2010). Additionally, downstream EPF-family peptides and receptors such as EPF1/EPF2 and ERECTA-family kinases interact to buffer stomatal density within a physiologically optimal range (Hara *et al.*, 2007, 2009; Hunt and Gray, 2009). The non-significant correlation observed here likely reflects this developmental complexity and the system's capacity to maintain SD homeostasis even with constitutive STO overexpression. In contrast, the highly significant positive correlation between STO expression and the number of clustered stomata indicated that increased STOMAGEN expression directly compromises spacing fidelity. This aligns with findings in *Arabidopsis*, where excess STOMAGEN has been shown to override EPF1-mediated spacing inhibition, resulting in the breakdown of the one-cell spacing rule (Sugano *et al.*, 2009; Tanaka *et al.*, 2013; Dow, Bergmann and Berry, 2014; Sakoda *et al.*, 2020). The disproportionately strong effect on clustering suggests that high STO expression does not merely increase stomatal number, but also disrupts spatial patterning, potentially impairing coordinated guard cell function and gas exchange regulation (Dow, Berry and Bergmann, 2014). These results imply that cluster formation is a more direct and sensitive developmental output of STOMAGEN overexpression, whereas SD is shaped by a broader, environmentally buffered signalling network.

Conversely, in the glasshouse-grown plants, the influence of transgene expression on stomatal density appeared markedly diminished. Notably, previously high-SD STOMAGEN genotypes, such as S_71, exhibited a significant reduction in stomatal density, suggesting that environmental factors (most notably sustained and sometimes extreme heat stress) may have overridden or suppressed transgene-driven effects on stomatal development. The glasshouse temperatures ranged from 25-55 °C, exceeding the optimum growth temperature of 18–24 °C for cultivated Strawberry (Gonzalez-Fuentes *et al.*, 2016), creating a thermal environment likely to elicit stress responses. This suggests that environmental stress may have overridden transgene-driven stomatal initiation, possibly through suppression of meristemoid proliferation or enhanced activity of inhibitory signals such as EPF2 or abscisic acid (ABA) (Pillitteri and Torii, 2012; Lau *et al.*, 2018). Moreover, such heat stress likely induced secondary drought stress via increased soil water evaporation, especially in the well-ventilated glasshouse, further modulating stomatal development. Drought and VPD are known to repress stomatal formation in developing leaves through systemic ABA signalling (Yoo *et al.*, 2012; Yoko Tanaka *et al.*, 2013), and may explain why some transgenic lines failed to maintain elevated SD despite high STOMAGEN expression. In hypostomatous species like strawberry, this may interact with inherent epidermal limits, leading to a developmental ceiling in stomatal number, particularly under combined heat and drought-like conditions caused by increased evapotranspirative demand and soil drying (Franks and Farquhar, 2007; Tanaka *et al.*, 2013).

While relative expression data for 35S::STO were available only from plants grown in the CT room, due to tissue loss from stress and mortality in the glasshouse, the significant correlation observed between STO expression and stomatal clustering in the CT environment remains biologically meaningful. Importantly, stomatal clustering remained evident in the glasshouse SD measurements (Fig. 3.4), even where total density stagnated, indicating that clustering defects persist under environmental stress. This suggests that the disruption of the one-cell spacing rule, mediated by STOMAGEN overexpression and likely saturation of the EPF1/TMM regulatory module, is a robust and less environmentally labile developmental outcome (Hara *et al.*, 2007;

Dow, Bergmann and Berry, 2014). The results presented here are consistent with the well-established plasticity of stomatal development in response to environmental conditions, as stomatal density was found to be sensitive to stress, suggesting that environmental suppression can override genetically driven increases in stomatal density (Farquhar and Sharkey, 1982; Grassi and Magnani, 2005; Xu and Zhou, 2008). In contrast, clustering represents a more stable phenotype of STO transgene activity. This has critical implications for genetic manipulation strategies: density gains may be limited by stress-induced suppression, but patterning disruptions may persist and impair gas exchange responsiveness, even when transgene expression is dampened by environmental override.

5.1.2.   Effect of transgenes on photosynthetic capacity

Changes in stomatal density and function have been shown to impact photosynthetic rates (Franks and Beerling, 2009; Wang *et al.*, 2013; Tanaka *et al.*, 2013; Dow, Berry and Bergmann, 2014; Lawson and Blatt, 2014; Antunes *et al.*, 2017; Caine *et al.*, 2019). Despite clear differences in stomatal development and patterning among transgenic lines, no significant differences were observed in photosynthetic capacity, including A_{max}, Vc_{max} and J_{max}. This was consistent across both KST1::HXK and 35S::STO overexpressing lines. These findings align with previous studies showing that genetic manipulation of stomatal traits alone is often insufficient to alter the biochemical parameters that limit photosynthesis (Kelly *et al.*, 2013; Tanaka *et al.*, 2013; Lugassi *et al.*, 2015).

Theoretically, increasing stomatal conductance (g_{sw}) may enhance CO_2 delivery and raise A_{max}, particularly under ambient CO_2 concentrations. However, in the present study, no lines displayed consistent increases in g_{sw}, and those with increased stomatal density (SD) often exhibited greater stomatal clustering, a condition previously shown to impair gas exchange efficiency and limit functional gains in photosynthesis (Dow, Berry and Bergmann, 2014). When accounting for the clustering, STOMAGEN lines S_261 and SH_15 have an effective SD

equivalent to the AZ (when counting stomata in a cluster as one functional unit), which may account for the lack of expected increase in g_{sw} and potential increase in A_{max}. Additionally, Vc_{max} and J_{max} are biochemical traits, reflecting Rubisco content and activity, and electron transport capacity, respectively, and are not typically influenced by stomatal traits unless sustained increases in carbon availability drive biochemical acclimation, a phenomenon not expected in the absence of enhanced sink demand or altered carbohydrate turnover (Lawson & Blatt, 2014).

Furthermore, the guard cell-specific overexpression of HXK, which promotes closure initiation in response to sugar accumulation, may indirectly reinforce carbon balance homeostasis and prevent overstimulation of photosynthetic enzymes (Kelly *et al.*, 2013; Lugassi *et al.*, 2015). Similarly, Tanaka et al. (2013) reported that changes in stomatal density mediated by STOMAGEN overexpression were not accompanied by shifts in photosynthetic capacity, supporting the idea that stomatal development and mesophyll biochemistry are often uncoupled, particularly in the absence of environmental drivers such as CO_2 enrichment or increased sink strength (Tanaka *et al.*, 2013). These results highlight the importance of considering source-sink coordination when interpreting or engineering photosynthetic traits and reinforce the notion that modifying stomatal traits alone does not necessarily lead to increased photosynthetic capacity.

5.1.3.   Effect of transgenes on stomatal behaviour

Stomatal density is one of the primary determinants of stomatal conductance, particularly the maximum stomatal conductance (g_{max}) (Lawson and Morison, 2004; Lawson, Caemmerer and Baroli, 2010; Drake, Froend and Franks, 2013). Genotypic differences in g_{sw} were most pronounced under low-light conditions preceding a step-increase in light intensity, with Hexokinase line H_354 exhibiting significantly higher g_{sw} than the azygous control and STOMAGEN lines. As measurements were conducted *ex-situ* in the early morning, before the onset of acute heat stress, the pretreatment differences likely reflect physiological carryover from the preceding day's conditions. Previous studies have shown that plants can exhibit "stomatal memory", maintaining

partial closure or altered stimuli sensitivity following stress exposure, and exposure to stress events can have persisting effects, even on newly developing leaves (Atkinson, Davies and Mansfield, 1989; Pospíšilová, 1996; Galmés *et al.*, 2007; Fanourakis *et al.*, 2011). Low g_{sw} under initial low light conditions in this context may, therefore, represent a conservative response to residual drought or thermal stress, potentially mediated by ABA accumulation or limited hydraulic recovery overnight (Skelton *et al.*, 2017; Li *et al.*, 2021). The observed differences between Hexokinase and STOMAGEN lines are consistent with their respective transgenic identities. Guard cell-specific overexpression of Hexokinase has previously shown enhanced drought tolerance and improved stomatal regulation under stress conditions in both controlled environments and field trials (Kelly *et al.*, 2019; Lugassi *et al.*, 2019; Acevedo-Siaca *et al.*, 2022). In contrast, STOMAGEN overexpression, which increases stomatal density but often results in clustering and reduced stomatal functionality, impairing aperture dynamics and increasing susceptibility to abiotic stress (Tanaka et al., 2013; Dow, Berry and Bergmann, 2014; Sakoda et al., 2020). The significantly lower g_{sw} in the STO line S_261 than the HXK line H_354 may therefore reflect dysfunctional stomatal behaviour under glasshouse conditions, compounded by residual stress effects from the previous photoperiod.

Stomatal clustering may impair stomatal function through disruptions of cell turgor, mechanical interference, impaired signalling coordination, and hydraulic limitations (Dow, Berry and Bergmann, 2014). While the glasshouse-grown strawberries showed no differences in SD, the gas exchange dynamics of the STOMAGEN overexpressing lines S_261 and SH_15 consistently trended towards lower g_{sw} throughout the step-changes in light intensity, particularly the STO single line S_261 (Fig. 3.12). While not statistically significant, this trend may corroborate the notion that clustered stomata may also suffer from reductions in the effective g_{sw} of the individuals present within the cluster due to boundary layer alterations (Dow, Berry and Bergmann, 2014). This finding supports previous observations that stomata within clusters often fail to operate independently, with impaired pore responsiveness and reduced contribution to effective conductance (Dow, Berry and Bergmann, 2014; Papanatsiou *et al.*, 2019). Clustering has been shown to disrupt the one-cell

spacing rule, which is essential for the correct propagation of signalling gradients (such as CO_2, light, and ABA) that mediate coordinated stomatal behaviour (Hara *et al.*, 2007, 2009; Zoulias *et al.*, 2018). These results highlight the importance of stomatal patterning, not just total density, in determining the physiological capacity for gas exchange, especially during dynamic environmental transitions and in genotypes with known spacing defects.

Stomatal behaviour and pore function regulate the real-time dynamics of *stomatal conductance* (Lawson et al., 1998; Dow, Berry and Bergmann, 2014; Takahashi et al., 2015). Both the speed and rate of stomatal response can limit CO_2 assimilation rate and reduce iWUE during opening and closure, respectively (Lawson and Blatt, 2014; Qu *et al.*, 2016, 2020; Lawson and Vialet-Chabrand, 2019; Long *et al.*, 2022). To further explore the effects of the transgenes on stomatal dynamics, stomatal conductance response curves were fit using the Vialet-Chabrand model, allowing derivation of key kinetic parameters: stomatal kinetics constant (k) and lag time (l) for stomatal opening and closure (Vialet-Chabrand *et al.*, 2017). In this framework, the lag time (l) represents the delay between an environmental change and the initiation of a measurable stomatal response, while the kinetics constant (k) describes the rate at which stomatal conductance approaches its new steady state once the response has begun (with smaller values indicating a faster kinetics) (Vialet-Chabrand *et al.*, 2017). No genotypic differences in k or l were found across stomatal opening or closure, suggesting that the transgenes had little to no effect on stomatal behaviour. A trend toward shorter lag time (l) during light stomatal closure, relative to stomatal opening, was observed across most genotypes, except for the STO-only line S_261. While not always statistically significant, this pattern was apparent even in the Azygous line (510s delay before significant stomatal opening vs ~106s delay before significant stomatal closure), suggesting that an asymmetric stomatal response to light transitions may represent an inherent physiological trait in strawberry. This interpretation is supported by observations from *Yokoyama et al. (2023)*, in which strawberry stomata were shown to close under relatively mild midday water stress, indicating a conservatively biased stomatal behaviour that may favour early closure to minimise water loss under fluctuating environmental conditions (Yokoyama *et al.*, 2023).

Notably, the double-expressing line, SH_15, exhibited a significantly reduced lag time before stomatal closure compared to opening, in contrast to the STO-only line. This divergence in response may reflect partial restoration of stomatal functionality by HXK, potentially through its role in sugar sensing and regulation of guard cell turgor. This interpretation is consistent with prior studies demonstrating that guard cell-specific expression of HXK can enhance closure dynamics and water-use efficiency without impairing photosynthesis, particularly under conditions of environmental stress (Kelly *et al.*, 2013, 2019; Lugassi *et al.*, 2015). Mechanistically, higher HXK activity in guard cells could reduce closure lag by amplifying ABA- and sugar-mediated signalling, effectively lowering the threshold for initiating ion efflux and turgor loss. In clustered stomata, where mechanical and spatial constraints can delay closure, this stronger signalling input may help overcome the sluggish onset of the response, allowing closure to begin more promptly even if the subsequent kinetics remain constrained (Kelly *et al.*, 2013, 2019; Lugassi *et al.*, 2015, 2019). However, this rescue of lag under clustered conditions does not equate to an enhancement of the innate rapid closure response in HXK single lines lacking clustering, where lag times remain similar to the control or are not significantly improved.

In addition, the double-expressing line was found to have fewer clustered stomata per mm² compared to the STOMAGEN-only line (39 and 56, respectively). The reduced incidence of clustering may also have contributed to the reduced lag time, as stomatal clustering has been previously associated with impaired responsiveness, reduced conductance, and aberrant pore behaviour (Dow, Berry and Bergmann, 2014). The findings presented here suggest that the impaired responsiveness observed in the STO-only line may result from both clustering-induced dysfunction and the absence of HXK-mediated regulatory control, whereas the double line may benefit from HXK-mediated compensation and reduced local interference among neighbouring stomata.

Together, these results point to a complex interaction between stomatal patterning and behaviour, in which hexokinase expression may rescue clustering-induced limitations in stomatal dynamics and support faster closure in response to declining light. The combination of a conserved kinetic

response with a trend toward faster closure further supports the view that strawberry may employ an intrinsically conservative stomatal strategy, likely evolved to prioritise water conservation under variable field conditions.

5.2.   Future applications

While few obvious benefits from the stomatal manipulations presented in this thesis are presented, the stomatal limitations to productivity and slow responsiveness remain (Lawson and Blatt, 2014; McAusland *et al.*, 2016). Thus, genetic manipulations of stomatal patterning and behaviour have the potential to alleviate these constraints. The data presented in this thesis are informative, examining understudied crop species and exploring suboptimal conditions, and can help guide future manipulation strategies.

In Strawberry, stomatal limitation is one of the major constraints to carbon assimilation, particularly after midday and under stressful conditions (Yokoyama *et al.*, 2023). Repression of the innate midday depression may allow strawberries to achieve greater cumulative carbon gain as well as dissipate heat stress, as temperatures can easily exceed optimal conditions when grown in polytunnels or glasshouses. One obvious manipulation may be guard cell-targeted RNA interference of the endogenous strawberry hexokinase. As this gene is shown to play a role in stomatal closure under optimal conditions, it may play a very strong role in the midday depression in strawberries (Kelly *et al.*, 2013; Yokoyama *et al.*, 2023). Reducing the expression of HXK may help to maintain higher g_{sw} throughout the afternoon, providing evaporative cooling and greater diurnal carbon gain. Evaporative cooling via higher stomatal conductance may alleviate heat-induced declines in photosynthetic efficiency by lowering leaf temperature. Heat stress in strawberry reduces net CO_2 assimilation, PSII efficiency, and biomass, particularly above 35-40 °C, with evidence of irreversible photodamage to the photosystems (Kadir, Sidhu and Al-Khatib, 2006; Kesici *et al.*, 2013; Menzel, 2024). Increased transpiration can help dissipate excess heat, reducing midday depression of photosynthesis, a phenomenon also demonstrated in other fruit crops such as cranberry, where evaporative cooling lowered leaf temperature by 5-10 °C and improved carbon gain (Pelletier *et al.*, 2016). While this inevitably comes at the cost of greater

water use, in strawberries grown in polytunnels or glasshouses under relatively controlled and irrigated conditions, the benefits of sustained photosynthesis, improved thermal tolerance, and greater diurnal carbon gain may outweigh the penalties in water-use efficiency.

Increasing the SD of strawberry remains an effective method of alleviating stomatal diffusional resistances. To avoid aberrant stomatal clustering phenotypes, as displayed here (Chapter 3), targeted knock-outs of competitive antagonist ligands from EPF1 and EPF2 could be employed. Sakoda et al. (2020) used the targeted knock-out of EPF1 to produce moderate increases in SD (~50%), which resulted in greater biomass accumulation than the WT or STOMAGEN overexpression (Sakoda *et al.*, 2020). The propensity for stomatal clustering in the 35S::STO strawberry lines produced here may suggest greater competition between STOMAGEN and EPF1 than between STOMAGEN and EPF2 for the binding of the ERECTA family receptors (ER, ERL1, ERL2) in complex with TMM, as EPF1 acts much later in development, acting to enforce the one-cell spacing rule (Hara *et al.*, 2007; Sugano *et al.*, 2009; Dow, Bergmann and Berry, 2014). Targeted KO of EPF1 in strawberry may, therefore, provide a way to increase SD moderately without incurring the extreme clustering penalties resulting from transgenic overexpression. Conventional breeding strategies, aimed at exploiting natural variation in STOMAGEN expression, which acts as a positive regulator of stomatal development, offer a mechanism to modulate stomatal density (SD) within agronomically useful ranges. Given that SD is a strongly heritable trait, identifying or selecting alleles of STOMAGEN (or its regulatory network) that promote a moderate increase in SD without inducing clustering could provide breeders with a route to enhance photosynthetic capacity. Such fine-tuning would allow greater CO_2 uptake under favourable conditions while retaining stomatal flexibility, helping to overcome one of the key bottlenecks to productivity in strawberry. Such an approach would offer a more precise means of enhancing stomatal conductance in strawberry, balancing gains in CO_2 diffusion with maintenance of functional stomatal patterning, and highlights the value of loss-of-function strategies in achieving more controlled trait improvements than constitutive overexpression.

6. References

Acevedo-Siaca, L.G. *et al.* (2022) 'Guard-cell-targeted overexpression of Arabidopsis Hexokinase 1 can improve water use efficiency in field-grown tobacco plants', *Journal of Experimental Botany*, 73(16), pp. 5745–5757. Available at: https://doi.org/10.1093/JXB/ERAC218.

Antunes, W.C. *et al.* (2017) 'Guard cell-specific down-regulation of the sucrose transporter SUT1 leads to improved water use efficiency and reveals the interplay between carbohydrate metabolism and K+ accumulation in the regulation of stomatal opening', *Environmental and Experimental Botany*, 135, pp. 73–85. Available at: https://doi.org/10.1016/J.ENVEXPBOT.2016.12.004.

Atkinson, C.J., Davies, W.J. and Mansfield, T.A. (1989) 'Changes in Stomatal Conductance in Intact Ageing Wheat Leaves in Response to Abscisic Acid', *Journal of Experimental Botany*, 40(9), pp. 1021–1028. Available at: https://doi.org/10.1093/JXB/40.9.1021.

Bergmann, D.C. and Sack, F.D. (2007) 'Stomatal Development', *Annual Review of Plant Biology*, 58, pp. 163–181. Available at: https://doi.org/10.1146/annurev.arplant.58.032806.104023.

Bhat, S.R. and Srinivasan, R. (2002) 'Molecular and genetic analyses of transgenic plants:: Considerations and approaches', *Plant Science*, 163(4), pp. 673–681. Available at: https://doi.org/10.1016/S0168-9452(02)00152-8.

Caine, R.S. *et al.* (2019) 'Rice with reduced stomatal density conserves water and has improved drought tolerance under future climate conditions', *New Phytologist*, 221(1), pp. 371–384. Available at: https://doi.org/10.1111/NPH.15344/FORMAT/PDF.

Casson, S. and Gray, J.E. (2008) 'Influence of environmental factors on stomatal development', *New Phytologist*, 178(1), pp. 9–23. Available at: https://doi.org/10.1111/J.1469-8137.2007.02351.X.

Casson, S.A. and Hetherington, A.M. (2010) 'Environmental regulation of stomatal development', *Current Opinion in Plant Biology*, 13(1), pp. 90–95. Available at: https://doi.org/10.1016/J.PBI.2009.08.005.

Crane, R. *et al.* (2023) 'Horticulture Production in England'.

Department for Environment, F. and R.A. *et al.* (2019) *Agriculture in the United Kingdom 2019*.

Available at:

https://assets.publishing.service.gov.uk/government/uploads/system/uploads/attachment_data/file/

950618/AUK-2019-07jan21.pdf (Accessed: 19 November 2021).

Dow, G.J., Bergmann, D.C. and Berry, J.A. (2014) 'An integrated model of stomatal development

and leaf physiology', *New Phytologist*, 201(4), pp. 1218–1226. Available at:

https://doi.org/10.1111/NPH.12608.

Dow, G.J., Berry, J.A. and Bergmann, D.C. (2014) 'The physiological importance of developmental

mechanisms that enforce proper stomatal spacing in Arabidopsis thaliana', *New Phytologist*,

201(4), pp. 1205–1217. Available at: https://doi.org/10.1111/NPH.12586.

Drake, P.L., Froend, R.H. and Franks, P.J. (2013) 'Smaller, faster stomata: scaling of stomatal

size, rate of response, and stomatal conductance', *Journal of Experimental Botany*, 64(2), pp. 495–

505. Available at: https://doi.org/10.1093/JXB/ERS347.

Dutton, C. *et al.* (2019) 'Bacterial infection systemically suppresses stomatal density', *Plant, Cell &*

Environment, 42(8), pp. 2411–2421. Available at: https://doi.org/10.1111/PCE.13570.

Fanourakis, D. *et al.* (2011) 'Avoiding high relative air humidity during critical stages of leaf

ontogeny is decisive for stomatal functioning', *Physiologia Plantarum*, 142(3), pp. 274–286.

Available at: https://doi.org/10.1111/J.1399-3054.2011.01475.X.

Farquhar, G.D. and Sharkey, T.D. (1982) 'Stomatal Conductance and Photosynthesis', *Annual*

Review of Plant Physiology, 33(1), pp. 317–345. Available at:

https://doi.org/10.1146/ANNUREV.PP.33.060182.001533.

Franks, P.J. and Beerling, D.J. (2009) 'Maximum leaf conductance driven by CO2 effects on

stomatal size and density over geologic time', *Proceedings of the National Academy of Sciences*,

106(25), pp. 10343–10347. Available at: https://doi.org/10.1073/PNAS.0904209106.

Franks, P.J. and Farquhar, G.D. (2007) 'The Mechanical Diversity of Stomata and Its Significance

in Gas-Exchange Control', *Plant Physiology*, 143(1), pp. 78–87. Available at:

https://doi.org/10.1104/PP.106.089367.

Galmés, J. *et al.* (2007) 'Water relations and stomatal characteristics of Mediterranean plants with different growth forms and leaf habits: Responses to water stress and recovery', *Plant and Soil*, 290(1–2), pp. 139–155. Available at: https://doi.org/10.1007/S11104-006-9148-6/FIGURES/8.

Geisler, M., Nadeau, J. and Sack, F.D. (2000a) 'Oriented Asymmetric Divisions That Generate the Stomatal Spacing Pattern in Arabidopsis Are Disrupted by the too many mouths Mutation', *The Plant Cell*, 12(11), pp. 2075–2086. Available at: https://doi.org/10.1105/TPC.12.11.2075.

Geisler, M., Nadeau, J. and Sack, F.D. (2000b) 'Oriented Asymmetric Divisions That Generate the Stomatal Spacing Pattern in Arabidopsis Are Disrupted by the too many mouths Mutation', *The Plant Cell*, 12(11), pp. 2075–2086. Available at: https://doi.org/10.1105/TPC.12.11.2075.

Gonzalez-Fuentes, J.A. *et al.* (2016) 'Diurnal root zone temperature variations affect strawberry water relations, growth, and fruit quality', *Scientia Horticulturae*, 203, pp. 169–177. Available at: https://doi.org/10.1016/J.SCIENTA.2016.03.039.

Grassi, G. and Magnani, F. (2005) 'Stomatal, mesophyll conductance and biochemical limitations to photosynthesis as affected by drought and leaf ontogeny in ash and oak trees', *Plant, Cell and Environment*, 28(7), pp. 834–849. Available at: https://doi.org/10.1111/J.1365-3040.2005.01333.X;JOURNAL:JOURNAL:13653040;REQUESTEDJOURNAL:JOURNAL:13653040;WGROUP:STRING:PUBLICATION.

Hamanishi, E.T., Thomas, B.R. and Campbell, M.M. (2012) 'Drought induces alterations in the stomatal development program in Populus', *Journal of Experimental Botany*, 63(13), pp. 4959–4971. Available at: https://doi.org/10.1093/JXB/ERS177.

Hara, K. *et al.* (2007a) 'The secretory peptide gene EPF1 enforces the stomatal one-cell-spacing rule', *Genes & Development*, 21(14). Available at: https://doi.org/10.1101/GAD.1550707.

Hara, K. *et al.* (2007b) 'The secretory peptide gene EPF1 enforces the stomatal one-cell-spacing rule', *Genes & Development*, 21(14), p. 1720. Available at: https://doi.org/10.1101/GAD.1550707.

Hara, K. *et al.* (2009) 'Epidermal Cell Density is Autoregulated via a Secretory Peptide, EPIDERMAL PATTERNING FACTOR 2 in Arabidopsis Leaves', *Plant and Cell Physiology*, 50(6), pp. 1019–1031. Available at: https://doi.org/10.1093/PCP/PCP068.

Hatfield, J.L. and Dold, C. (2019) 'Water-use efficiency: Advances and challenges in a changing climate', *Frontiers in Plant Science*, 10, p. 103. Available at: https://doi.org/10.3389/FPLS.2019.00103/BIBTEX.

Hunt, L. and Gray, J.E. (2009) 'The signaling peptide EPF2 controls asymmetric cell divisions during stomatal development', *Current biology : CB*, 19(10), pp. 864–869. Available at: https://doi.org/10.1016/J.CUB.2009.03.069.

Kelly, G. *et al.* (2013) 'Hexokinase mediates stomatal closure', *The Plant journal : for cell and molecular biology*, 75(6), pp. 977–988. Available at: https://doi.org/10.1111/TPJ.12258.

Kelly, G. *et al.* (2019) 'Guard-Cell Hexokinase Increases Water-Use Efficiency Under Normal and Drought Conditions', *Frontiers in Plant Science*, 10, p. 1499. Available at: https://doi.org/10.3389/FPLS.2019.01499/BIBTEX.

Kirkham, M.B. (2005) 'Principles of Soil and Plant Water Relations', *Principles of Soil and Plant Water Relations* [Preprint]. Available at: https://doi.org/10.1016/B978-0-12-409751-3.X5000-2.

Kirkham, M.B. (2014) 'Principles of soil and plant water relations, 2nd Edition', *Principles of Soil and Plant Water Relations, 2nd Edition*, pp. 1–579. Available at: https://doi.org/10.1016/C2013-0-12871-1.

Lake, J.A., Woodward, F.I. and Quick, W.P. (2002) 'Long-distance CO2 signalling in plants', *Journal of Experimental Botany*, 53(367), pp. 183–193. Available at: https://doi.org/10.1093/JEXBOT/53.367.183.

LaMondia, J.A. (2004) 'Strawberry black root rot', *Advances in strawberry research*, 23, pp. 1–10.

Lau, O.S. *et al.* (2018) 'Direct Control of SPEECHLESS by PIF4 in the High-Temperature Response of Stomatal Development', *Current Biology*, 28(8), pp. 1273-1280.e3. Available at: https://doi.org/10.1016/J.CUB.2018.02.054.

Lawson, T. *et al.* (2014) 'Mesophyll photosynthesis and guard cell metabolism impacts on stomatal behaviour', *New Phytologist*, 203(4), pp. 1064–1081. Available at: https://doi.org/10.1111/NPH.12945.

Lawson, T. and Blatt, M.R. (2014) 'Stomatal Size, Speed, and Responsiveness Impact on Photosynthesis and Water Use Efficiency', *Plant Physiology*, 164(4), pp. 1556–1570. Available at: https://doi.org/10.1104/PP.114.237107.

Lawson, T., Caemmerer, S. von and Baroli, I. (2010) 'Photosynthesis and Stomatal Behaviour', pp. 265–304. Available at: https://doi.org/10.1007/978-3-642-13145-5_11.

Lawson, T. and Morison, J.I.L. (2004a) 'Stomatal function and physiology', *The Evolution of Plant Physiology*, pp. 217–242. Available at: https://doi.org/10.1016/B978-012339552-8/50013-5.

Lawson, T. and Morison, J.I.L. (2004b) 'Stomatal function and physiology', *The Evolution of Plant Physiology: From whole plants to ecosystems*, pp. 217–242. Available at: https://doi.org/10.1016/B978-012339552-8/50013-5.

Lawson, T. and Vialet-Chabrand, S. (2019) 'Speedy stomata, photosynthesis and plant water use efficiency', *New Phytologist*, 221(1), pp. 93–98. Available at: https://doi.org/10.1111/NPH.15330.

Lawson, T., Weyers, J. and Brook, R.A.' (1998) 'The nature of heterogeneity in the stomatal behaviour of Phaseolus vulgaris L. primary leaves', *Journal of Experimental Botany*, 49(325), pp. 1387–1395. Available at: https://academic.oup.com/jxb/article/49/325/1387/506284 (Accessed: 24 April 2025).

Li, S. *et al.* (2021) 'Role of Hydraulic Signal and ABA in Decrease of Leaf Stomatal and Mesophyll Conductance in Soil Drought-Stressed Tomato', *Frontiers in Plant Science*, 12, p. 653186. Available at: https://doi.org/10.3389/FPLS.2021.653186/FULL.

Long, S.P. *et al.* (2022) 'Into the Shadows and Back into Sunlight: Photosynthesis in Fluctuating Light', *Annual Review of Plant Biology*, 73(Volume 73, 2022), pp. 617–648. Available at: https://doi.org/10.1146/ANNUREV-ARPLANT-070221-024745/CITE/REFWORKS.

Lugassi, N. *et al.* (2015) 'Expression of Arabidopsis Hexokinase in Citrus Guard Cells Controls Stomatal Aperture and Reduces Transpiration', *Frontiers in Plant Science*, 0(DEC), p. 1114. Available at: https://doi.org/10.3389/FPLS.2015.01114.

Lugassi, N. *et al.* (2019) 'Expression of Arabidopsis Hexokinase in Tobacco Guard Cells Increases Water-Use Efficiency and Confers Tolerance to Drought and Salt Stress', *Plants*, 8(12). Available at: https://doi.org/10.3390/plants8120613.

Mano, N.A., Madore, B. and Mickelbart, M. V. (2023) 'Different Leaf Anatomical Responses to Water Deficit in Maize and Soybean', *Life*, 13(2), p. 290. Available at: https://doi.org/10.3390/LIFE13020290/S1.

Nadeau, J.A. (2009) 'Stomatal development: new signals and fate determinants', *Current Opinion in Plant Biology*, 12(1), pp. 29–35. Available at: https://doi.org/10.1016/J.PBI.2008.10.006.

Nadeau, J.A. and Sack, F.D. (2002) 'Control of stomatal distribution on the Arabidopsis leaf surface', *Science (New York, N.Y.)*, 296(5573), pp. 1697–1700. Available at: https://doi.org/10.1126/SCIENCE.1069596.

Nunes, T.D.G. *et al.* (2022) 'Quantitative effects of environmental variation on stomatal anatomy and gas exchange in a grass model', *Quantitative Plant Biology*, 3, p. e6. Available at: https://doi.org/10.1017/QPB.2021.19.

Ouyang, W. *et al.* (2017) 'Stomatal conductance, mesophyll conductance, and transpiration efficiency in relation to leaf anatomy in rice and wheat genotypes under drought', *Journal of Experimental Botany*, 68(18), pp. 5191–5205. Available at: https://doi.org/10.1093/JXB/ERX314.

Papanatsiou, M. *et al.* (2019) 'Optogenetic manipulation of stomatal kinetics improves carbon assimilation,water use, and growth', *Science*, 363(6434), pp. 1456–1459. Available at: https://doi.org/10.1126/SCIENCE.AAW0046/SUPPL_FILE/AAW0046_PAPANATSIOU_SM.PDF.

Pillitteri, L.J. and Torii, K.U. (2012) 'Mechanisms of stomatal development', *Annual Review of Plant Biology*, 63(Volume 63, 2012), pp. 591–614. Available at: https://doi.org/10.1146/ANNUREV-ARPLANT-042811-105451/CITE/REFWORKS.

Pospíšilová, J. (1996) 'Effect of air humidity on the development of functional stomatal apparatus', *Biologia Plantarum*, 38(2), pp. 197–204. Available at: https://doi.org/10.1007/BF02873846/METRICS.

Qu, M. *et al.* (2016) 'Rapid stomatal response to fluctuating light: an under-explored mechanism to improve drought tolerance in rice', *Functional Plant Biology*, 43(8), pp. 727–738. Available at: https://doi.org/10.1071/FP15348.

Qu, M. *et al.* (2020) 'Alterations in stomatal response to fluctuating light increase biomass and yield of rice under drought conditions', *The Plant Journal*, 104(5), pp. 1334–1347. Available at: https://doi.org/10.1111/TPJ.15004.

Sakoda, K. *et al.* (2020) 'Higher Stomatal Density Improves Photosynthetic Induction and Biomass Production in Arabidopsis Under Fluctuating Light', *Frontiers in Plant Science*, 0, p. 1609. Available at: https://doi.org/10.3389/FPLS.2020.589603.

Schnell, J. *et al.* (2014) 'A comparative analysis of insertional effects in genetically engineered plants: considerations for pre-market assessments', *Transgenic Research*, 24(1), p. 1. Available at: https://doi.org/10.1007/S11248-014-9843-7.

Shpak, E.D. *et al.* (2005) 'Stomatal patterning and differentiation by synergistic interactions of receptor kinases', *Science (New York, N.Y.)*, 309(5732), pp. 290–293. Available at: https://doi.org/10.1126/SCIENCE.1109710.

Skelton, R.P. *et al.* (2017) 'Gas exchange recovery following natural drought is rapid unless limited by loss of leaf hydraulic conductance: evidence from an evergreen woodland', *New Phytologist*, 215(4), pp. 1399–1412. Available at: https://doi.org/10.1111/NPH.14652.

Sugano, S.S. *et al.* (2010) 'Stomagen positively regulates stomatal density in Arabidopsis', *Nature*, 463(7278), pp. 241–244. Available at: https://doi.org/10.1038/NATURE08682.

Takahashi, S. *et al.* (2015) 'Natural Variation in Stomatal Responses to Environmental Changes among Arabidopsis thaliana Ecotypes', *PLOS ONE*, 10(2), p. e0117449. Available at: https://doi.org/10.1371/JOURNAL.PONE.0117449.

Tanaka, Yoko *et al.* (2013) 'ABA inhibits entry into stomatal-lineage development in Arabidopsis leaves', *The Plant Journal*, 74(3), pp. 448–457. Available at: https://doi.org/10.1111/TPJ.12136.

Tanaka, Y *et al.* (2013) 'Enhancement of leaf photosynthetic capacity through increased stomatal density in Arabidopsis', *The New phytologist*, 198(3), pp. 757–764. Available at: https://doi.org/10.1111/NPH.12186.

Vialet-Chabrand, S.R.M. *et al.* (2017) 'Temporal Dynamics of Stomatal Behavior: Modeling and Implications for Photosynthesis and Water Use', *Plant Physiology*, 174(2), pp. 603–613. Available at: https://doi.org/10.1104/PP.17.00125.

Wang, Y. *et al.* (2013) 'Overexpression of plasma membrane H+-ATPase in guard cells promotes light-induced stomatal opening and enhances plant growth', *Proceedings of the National Academy of Sciences of the United States of America*, 111(1), pp. 533–538. Available at: https://doi.org/10.1073/PNAS.1305438111/SUPPL_FILE/PNAS.201305438SI.PDF.

Wong, S.C., Cowan, I.R. and Farquhar, G.D. (1979) 'Stomatal conductance correlates with photosynthetic capacity', *Nature 1979 282:5737*, 282(5737), pp. 424–426. Available at: https://doi.org/10.1038/282424a0.

Xu, Z. and Zhou, G. (2008a) 'Responses of leaf stomatal density to water status and its relationship with photosynthesis in a grass', *Journal of Experimental Botany*, 59(12), pp. 3317–3325. Available at: https://doi.org/10.1093/JXB/ERN185.

Xu, Z. and Zhou, G. (2008b) 'Responses of leaf stomatal density to water status and its relationship with photosynthesis in a grass', *Journal of Experimental Botany*, 59(12), p. 3317. Available at: https://doi.org/10.1093/JXB/ERN185.

Yokoyama, G. *et al.* (2023) 'Diurnal changes in the stomatal, mesophyll, and biochemical limitations of photosynthesis in well-watered greenhouse-grown strawberries', *Photosynthetica*, 61(1), pp. 1–12. Available at: https://doi.org/10.32615/PS.2023.001.

Yoo, C.Y. *et al.* (2012) 'The Arabidopsis GTL1 Transcription Factor Regulates Water Use Efficiency and Drought Tolerance by Modulating Stomatal Density via Transrepression of SDD1', *The Plant Cell*, 22(12), pp. 4128–4141. Available at: https://doi.org/10.1105/TPC.110.078691.

Zoulias, N. *et al.* (2018) 'Molecular control of stomatal development', *Biochemical Journal*, 475(2), p. 441. Available at: https://doi.org/10.1042/BCJ20170413.